Engineering Structures 328 (2025) 119732

Contents lists available at ScienceDirect

Engineering Structures

journal homepage: www.elsevier.com/locate/engstruct

Cyclic behaviour of GFRP-RC precast column-cap beam frame assembly: A finite element investigation

Mohamed H. El-Naqeeb [a,b,1], Reza Hassanli [a,*,2], Yan Zhuge [a,3], Xing Ma [a,4], Milad Bazli [c,5], Allan Manalo [d,6]

[a] University of South Australia, UniSA STEM, Mawson Lakes, SA 5095, Australia
[b] Badr University in Cairo, School of Engineering and Technology, Cairo 11829, Egypt
[c] Faculty of Science and Technology, Charles Darwin University, Darwin, Australia
[d] Center for Future Materials, School of Engineering, University of Southern Queensland, QLD 4350, Australia

ARTICLE INFO

Keywords:
Connection details
Cyclic loading
Finite element model
GFRP
Precast concrete

ABSTRACT

The applications of glass fibre reinforced polymers (GFRPs) in reinforced concrete frames made up of precast elements have remained limited because of a limited understanding of their behaviour and the substantial challenges associated with testing large-scale structures. To bridge this knowledge gap, a detailed finite element model was developed and verified against a large-scale precast GFRP-RC frame assembled previously using epoxy resin and tested under cyclic loads. This was followed by a comprehensive parametric study to understand the effect of different parameters such as the material of connecting reinforcement, and section failure control (Tension/Compression) on the cyclic performance of GFRP-RC frames assembled out of individual precast GFRP-RC elements. Comparisons have also been made with respect to the steel-RC counterpart frames. It was found that the mechanical properties of the material of connecting reinforcement (dowels) with the same amount of reinforcement, determine the cyclic behaviour of precast GFRP-RC frames in terms of capacity, stiffness, energy dissipation, and residual damage. The use of mild stainless-steel dowels improved the energy dissipation capacity of the frame while high-strength stainless steel, GFRP and CFRP dowels contributed to minimum residual deformations. Therefore, the selection of connection reinforcement material relies on whether energy dissipation or minimum damage is prioritized. Compared with precast steel-RC frames with the same reinforcement ratio, the GFRP-RC frames exhibited better residual damage performance while exhibiting lower stiffness and energy dissipation. Among different connection details, the frame with epoxy-filled ducts located at the cap beam achieved the greatest lateral capacity. However, this was accompanied by a sudden failure resulting from tension control failure, which changed to a gradual concrete compression failure with increasing reinforcement amount. This study concluded that precast GFRP-RC frames controlled by concrete compression failure and assembled through epoxy-filled ducts located at the cap beam can achieve a comparable performance to the counterpart precast steel-RC frames in terms of initial stiffness and energy dissipation. Also, it can achieve a similar performance to the equivalent cast-in-place counterpart.

* Corresponding author.
E-mail addresses: mohamed.el-naqeeb@mymail.unisa.edu.au, mohamed.hafez@buc.edu.eg (M.H. El-Naqeeb), reza.hassanli@unisa.edu.au (R. Hassanli), yan.zhuge@unisa.edu.au (Y. Zhuge), xing.ma@unisa.edu.au (X. Ma), milad.bazli@cdu.edu.au (M. Bazli), allan.manalo@usq.edu.au (A. Manalo).
[1] https://orcid.org/0000-0002-0573-2978
[2] https://orcid.org/0000-0001-5855-6405
[3] https://orcid.org/0000-0003-1620-6743
[4] https://orcid.org/0000-0001-5488-5252
[5] https://orcid.org/0000-0001-9027-6155
[6] https://orcid.org/0000-0003-0493-433X

https://doi.org/10.1016/j.engstruct.2025.119732
Received 7 July 2024; Received in revised form 19 December 2024; Accepted 15 January 2025
Available online 22 January 2025
0141-0296/© 2025 The Author(s). Published by Elsevier Ltd. This is an open access article under the CC BY license (http://creativecommons.org/licenses/by/4.0/).

1. Introduction

Glass fibre reinforced polymers (GFRPs) have emerged as an effective reinforcement alternative to steel in construction. Due to their noncorrodible nature, high strength-to-weight ratio, electromagnetic transparency, and durability [1], GFRP have found extensive applications in different structures, especially in harsh environment [2]. This can enhance the long-term performance of reinforced concrete (RC) structures [3], and achieve considerable long-term savings [4] by reducing the large costs needed for corrosion repair [5]. On the other hand, GFRP bar behaves linearly elastic up to its ultimate tensile strength. It also has potentially lower transverse shear strength and relatively lower stiffness compared to steel reinforcement. The inherent differences between GFRP and steel bars give rise to the distinct structural behaviour of reinforced concrete (RC) elements with GFRP compared to steel-RC elements.

The behaviour of GFRP-RC frame structural systems in cast-in-place construction, including beams, columns, slabs, and connections, has been adequately investigated. It was found that GFRP-RC beams exhibit larger deflection than those with steel reinforcement due to the lower modulus of elasticity of GFRP than steel at the same reinforcement ratio [6]. The deflection can be controlled by increasing the reinforcement ratio [7] and conforming to the serviceability limit for GFRP-RC beams [7–9]. In columns, it was reported that longitudinal GFRP bars could resist compression stress of more than 700 MPa and provide good confinement as lateral reinforcement [10]. A minimum longitudinal GFRP reinforcement ratio of 1 % was defined as practical; however, increasing the reinforcement ratio to 2.5 % enhances the post-peak behaviour of the column [11]. Moreover, under the cyclic load, GFRP-RC columns exhibit gradual failure despite the brittle nature of GFRP bars [12]. The detailing of GFRP cross-ties and spirals plays a key role in the achieved cyclic performance of columns in terms of lateral strength and deformability [13], whereas the use of ultra-high-performance concrete enhances their cyclic performance in terms of stiffness and energy dissipation [14]. Proper connection design between columns and beams is essential to achieve the integrity and safety of the structure [15,16]. Plenty of studies have investigated the effect of different parameters affecting the cyclic performance of connections [17], including anchorage detailing [18], connection reinforcement [19], beam-to-column flexural ratio [20], slab [21] and lateral beams contribution [22]. The overall performance of frames was also previously evaluated [23,24]. Results of studies on cast-in-place connections came with suggested estimations for the design capacity for interior [20] and exterior connections [25,26] to prevent catastrophic brittle failure of connections in frames and ensure acceptable performance.

Although many studies have focused on the behaviour of connections in cast-in-place GFRP-RC structures, research and application of GFRP in precast concrete are limited. Precast concrete structures can offer many benefits, including fast construction, reduced on-site safety and health risks, and improved concrete production quality [27]. Fibre-reinforced polymers (FRPs), with their low weight-to-strength ratio, can be more attractive for precast construction due to the benefits of easier transportation and assembly, especially in structures in aggressive environments like jetties, where cast-in-place concrete can be challenging. Research at the University of South Australia has investigated the behaviour of beam-column connections in precast concrete structures in the last three years. The cyclic behaviour of beam-column sub-assemblies utilizing pocket and pocketless connections was experimentally investigated [28,29]. The results confirmed that pocketless connections utilizing post-installed epoxy anchored reinforcement outperformed those with pocket connections in terms of capacity, stiffness, and energy dissipation [28,29]. The pocket connection filled with epoxy experienced premature failure at the pocket corners due to stress concentration and insufficient column embedded length. To overcome this problem, it was suggested that the embedded length of the column should be at least 1.4 times the column thickness [30]. Meanwhile, the optimum detailing for pocketless connections using epoxy can be achieved using reinforcement of embedded length 25 times the bar diameter [31]. At the structure scale, two full-scale frames were tested under cyclic loads, one with pocket connections and the other with pocketless connections [32,33]. It was also found that the frame with pocketless connections achieved better cyclic performance in terms of capacity, stiffness, and energy dissipation.

Studies examining the cyclic behaviour of precast GFRP-RC large-scale frames are notably scarce, with only two full-scale frames examined in existing literature [32,33]. Both frames were case studies of jetty structures, where GFRP efficiently mitigates corrosion problems. Precast GFRP-RC columns and cap beams were used in both frames, with differences in the assembly methods. In the first frame, the precast elements were assembled through pockets filled with epoxy resin in the cap beam, requiring the beam size to exceed the column size to accommodate the columns, as seen in jetty designs. Premature failure was observed around the pockets due to insufficient depth, indicating the need for larger beam depths. To address this issue, a second frame was designed with typical geometry, using epoxied GFRP reinforcement through prefabricated ducts in both the beam and column for connections. The results of the second frame demonstrated significant improvements in cyclic behaviour compared to the first frame with pocket connections. However, there is a lack of comparative analyses with counterparts such as cast-in-place and/or steel-RC frames. These studies also did not thoroughly investigate the effect of different connection details. This knowledge gap is due to the considerable challenges and costs associated with conducting experimental tests on large-scale structures, along with inherent limitations in testing methodologies. Subsequently this leaves the cyclic behaviour of precast GFRP-RC frames unclear, thus hindering their practical application. To address this point, this study employs finite element analysis (FEA) to study the cyclic behaviour of precast GFRP-RC frames. A calibrated model for a large-scale frame assembly from the literature was employed to study the cyclic performance of such frames with different connection details as well as compare the performance with steel-RC counterparts frames. The study aims to provide a comprehensive understanding of the cyclic performance of precast GFRP-RC frames, thereby aiding in the selection of optimal connection techniques to enhance their performance.

2. Description of the finite element model

Abaqus [34] was employed to develop a finite element model (FEM) for analysing the nonlinear behaviour of precast GFRP-RC frames. The test setup of the large-scale frame tested under cyclic load by [32] was used for model verification and is shown in Fig. 1. The frame consists of two precast columns and two precast beams reinforced with GFRP bars and is connected by post-installed reinforcement through prefabricated ducts of diameter 38 mm. After casting the precast columns and beams, epoxy resin was used to bond the post-installed reinforcement to achieve structural integrity. Epoxy was used to accelerate the erection process which is an ongoing challenge the industry is facing. Epoxy has a higher early strength than conventional grout and requires less curing time as well as a high bond strength. A gap between the bottom beam and the strong floor was ensured using three steel plates to elevate the beam which enabled the beam to freely rotate. The load was applied horizontally to the top beam as shown in Fig. 1.

A total of six connection reinforcements were used at the upper connections, each with a diameter of 20 mm, whereas four connection reinforcements of 19 mm diameter were used at the bottom connections. The length of all connection reinforcements was the same, measuring 820 mm, with 420 mm embedded inside the beam and 400 mm inside the column. The precast elements were cast using ready-mix concrete. The concrete mix proportions are listed in Table 1. Standard cylinders measuring 100 × 200 mm (Diameter × Length) were tested to determine the actual properties of the concrete. The average compressive

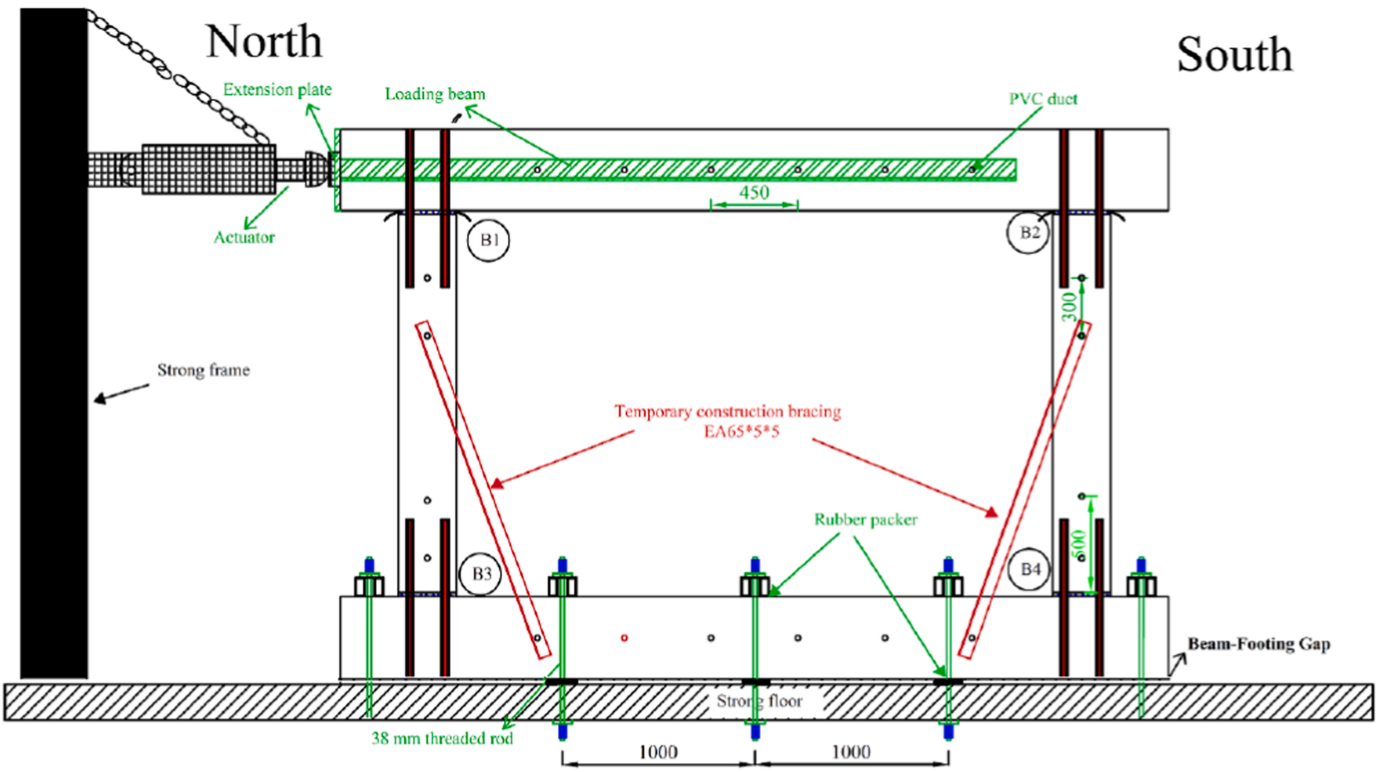

Fig. 1. Tested precast frame [32].

Table 1
Concrete mix design.

Cement (kg)	Fly ash (kg)	Aggregate (kg)	Sand (kg)	Water (kg)	Water reducer (L)	Retarder (L)
350	450	992	710	190	2.8	0.35

Table 2
Properties of the GFRP materials [32].

Bar No.	Modulus of Elasticity (GPa)	Ultimate Tensile Strength (MPa)	Ultimate strain in tension (ε_{fu})
# 10	62.50	1315	0.023
# 13	61.30	1282	0.021
# 16	60.00	1237	0.021
# 19	60.50	1270	0.021
#20	46.20	625	0.015

strength was found to be 82.5 MPa, and the modulus of elasticity was 39.5 GPa. The average compressive strength and modulus of elasticity of epoxy resin were 93.9 MPa, and 2300 MPa, respectively. The cross-section details of the precast column and beam, as well as the arrangement of connection reinforcement, are shown in Fig. 2. The properties of the GFRP reinforcement are listed in Table 2. Further details can be found in [32].

Fig. 3 shows the geometric FEM for the tested frame. To reduce the analysis time, a cutting plane in the XY plane (highlighted in red in Fig. 4) passing through the middle of the cross-sections of the beams and columns (see Fig. 2) was used to model only half of the frame geometry, taking advantage of symmetrical conditions. The geometric model consisted of four concrete solid components, each containing voids that represented the prefabricated circular ducts. The connection reinforcement was modelled as solid elements positioned at the centre of these ducts. To simulate the epoxy resin poured into the ducts, solid hollow elements were created to fill the remaining space around the reinforcement bars. This approach enabled a realistic simulation of the connection by assigning the mechanical properties of the epoxy resin to these solid elements. Additionally, adhesive properties between the

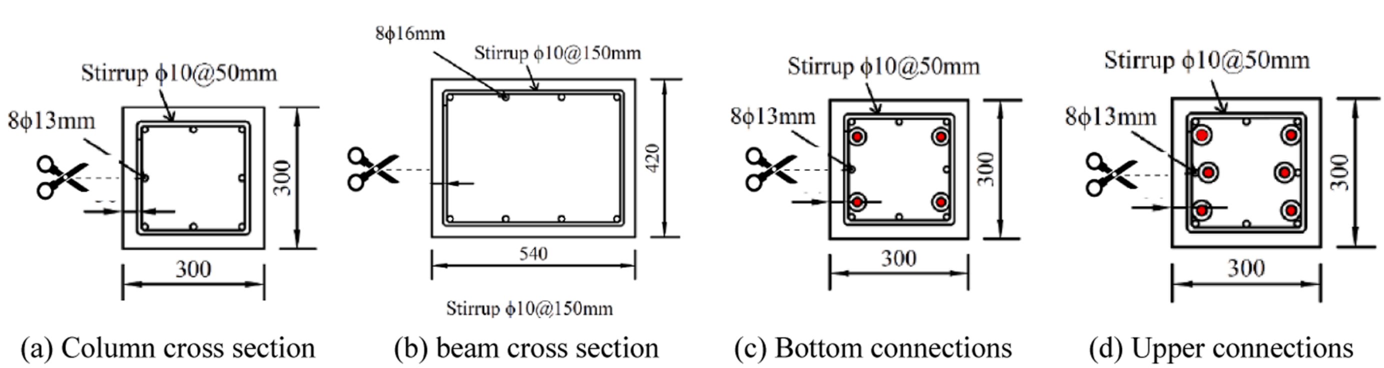

Fig. 2. Cross section details of frame parts [32].

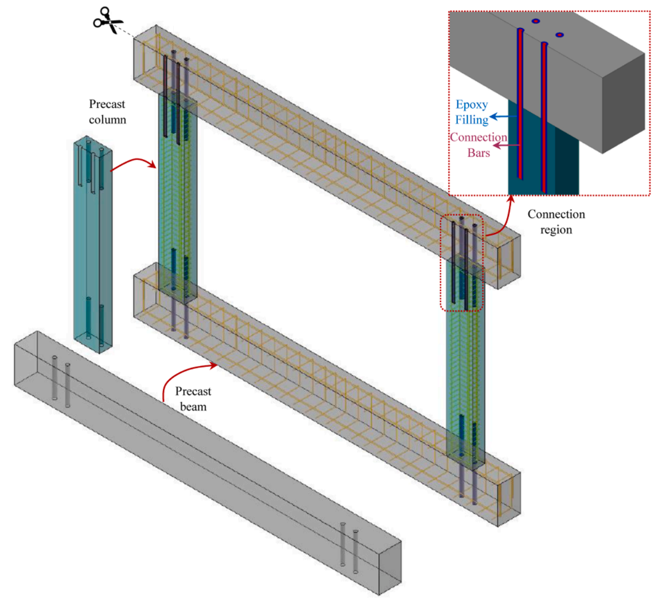

Fig. 3. Geometric finite element model.

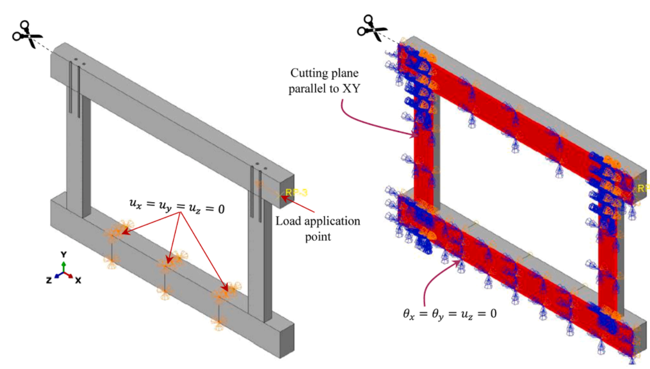

Fig. 4. Boundary condition and applied load.

contacting surfaces were defined using cohesive interaction, ensuring an accurate representation of the bond behaviour. Further details about the interaction properties and their implementation are discussed later. The boundary conditions due to symmetry for the rotations, θ and displacement, u ($\theta_x = \theta_y = u_z = 0$), as well as the boundary conditions at the clamping points ($u_x = u_y = u_z = 0$), are shown in Fig. 4. The displacement control cyclic load was applied to a reference point (located in the middle of the top beam cross-section) that interacted with the beam cross-section using a coupling constraint to avoid stress concentration.

The solid parts of concrete, connection reinforcement, and epoxy were modelled using the eight-nodded hexahedral C3D8R element. This element has three degrees of freedom at each node with reduced integration and the hourglass control option. The reinforcement of the precast columns and beams was modelled using the T3D2 truss element. The truss element has two nodes with three degrees of freedom at each node. The use of fine mesh size is essential for achieving accurate results that closely align with experimental data. However, this comes at the cost of significant computational time, creating a challenge to balance accuracy with reasonable running times. Initial trials were conducted with various mesh sizes using hexahedral elements to determine the optimum mesh size, particularly for the connection region, which is the most critical part due to higher strain concentrations. During these trials, larger mesh sizes resulted in convergence issues, causing the simulation to terminate until an optimal mesh size was identified for the connection region. To improve the convergence, a small viscosity parameter was employed in the Concrete Damage Plasticity (CDP) model. This approach not only improved convergence but also minimized the mesh size effect when the mesh size was reasonable [35]. Despite achieving convergence, using a uniform fine mesh size for the entire frame resulted in prohibitively long simulation times. To address this, the mesh size was increased in regions away from the connection, where stress and strain demands are less critical. The adopted meshing strategy utilized a fine mesh size in critical regions of the frame, such as the connections, while applying a coarser mesh size in the middle of the elements further from these regions. To ensure compatibility between fine and coarse mesh regions, transitional elements (C3D10) were used. The mesh distribution and transition approach are illustrated in Fig. 5, demonstrating the balance achieved between computational efficiency and simulation accuracy. These elements are ten-nodded quadratic tetrahedron elements. The total number of variables in the model, including elements and nodes, was 73542. The time increment was set to automatic, with a minimum time increment set to 10^{-15} to overcome non-convergence issues due to the many contacts defined, and the maximum time increment was 0.1 to speed up the simulation when possible.

The interaction between the several parts was taken according to [31], which presented a well-calibrated finite element model for precast GFRP-RC connections using epoxy resin for anchoring at the element scale. The reinforcement of the beam and column was modelled as embedded wires within the concrete elements, with common nodes sharing the same displacements. The interaction between the contacted surfaces of the beam and column was modelled by using Coulomb interaction through the coefficient of friction in the tangential direction and hard contact in the normal direction. Cohesive interaction was employed to model the interaction between epoxy and concrete or connection reinforcement to account for slippage. As reported in [31], the bond strength of epoxy anchored bar τ can be estimated according to Eq. (1). This available formula from the literature was developed for epoxy-anchored bars [36], effectively accounts for key parameters such as the bar's embedded length l_b, bar diameter d_b, concrete strength f_c:, as well as modulus of elasticity for both epoxy E_{ep} and bar E_b.

$$\tau = 0.59 l_b^{-0.32} d_b^{-0.59} E_b^{0.23} E_{ep}^{0.52} f_c^{0.31} \tag{1}$$

The behaviour of the concrete elements was defined using the concrete damage plasticity model (CDPM). This model effectively simulates the behaviour of concrete under compression and tension, considering concrete cracking and crushing as the governing failure modes. The behaviour of concrete under compression and tension was introduced according to the models developed by [37] and [38], respectively (see Fig. 6). The model's plasticity parameters are listed in Table 3. The parameters were taken according to [31] except for the viscosity

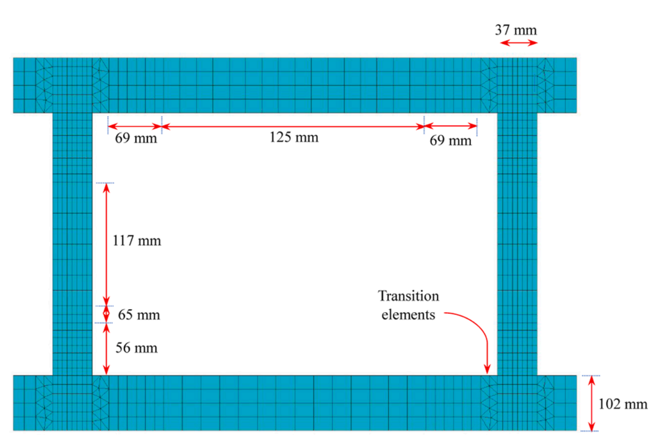

Fig. 5. Meshing of the frame.

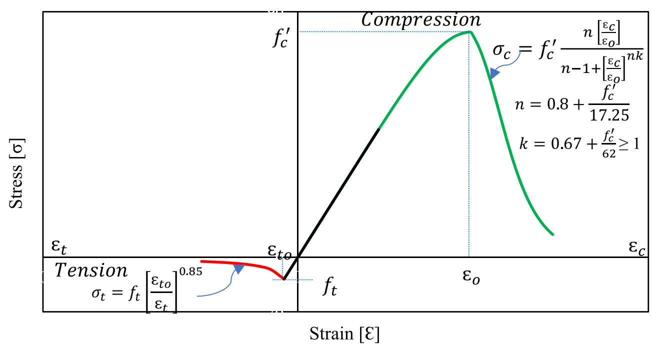

Fig. 6. Behaviour of concrete material [37], [38].

Table 3
Employed values for plasticity parameters in concrete damage plasticity model.

Parameter	Value	Definition
Dilation angle, ψ	36	Describes the inclination of the asymptote of the failure surface with respect to the hydrostatic axis, measured in the meridian plane
Eccentricity, ε	0.1	Describes the rate at which the potential flow function approaches the asymptote.
K_c	2/3	Defines the failure surface shape in the deviatoric cross section which considered a shape of three mutually tangent ellipses.
σ_{bo}/σ_{co}	1.16	The ratio between the biaxial concrete strength σ_{bo} to the uniaxial concrete strength σ_{co}.
Viscosity parameter, μ	0.00001	Parameter used to overcome convergence problems and reduce mesh size effect

parameter. A small value of the viscosity parameter is used to overcome non-convergence issues usually associated with modelling materials with strain-softening behaviour and using cohesive interaction [34]. Since the increment size was set to automatic, this value was set to the value listed in Table 2 after initial trials. It should be noted that the model needed 7376 increments to complete the simulation. According to [31], CPDM was also used to introduce the stress-strain behaviour of epoxy from the test. Moreover, the GFRP reinforcement was modelled as linear elastic up to its maximum tensile strength.

3. Calibration of the finite element model

The experimentally tested precast frame represented a column-to-cap beam assembly in jetty structures, where GFRP provided a solution to mitigate corrosion issues. The frame geometry was designed to be identical to a conventional jetty frame assembled using epoxy-filled pocket connections. This design requires a larger cap beam compared to the column to create pockets for the column embedded length. While the frame with pocket connections experienced premature failure and demonstrated weak performance, the tested frame was specifically designed to overcome these shortcomings [33]. The connection details, involving straight bars passing through the prefabricated ducts in both the cap beam and column, were designed to eliminate the presence of reinforcement protruding from the precast elements. This approach facilitates easier assembly of the structure and reduces the risk of damage to the bars during handling. Consequently, all connection reinforcement is inserted on-site. The amount of connection reinforcement was designed to ensure that the cross-section at the interface between the column and cap beam can achieve a flexural capacity equivalent to that of the column, thereby preventing local failure at the connection. The effect of the position of the connection reinforcement and its modulus of elasticity was carefully considered in the precise calculations. Epoxy resin was chosen as the anchoring material due to its specific properties for the target application, such as minimal shrinkage, high early strength, and excellent bonding capacity. These attributes enable the early use of the structure and reduce the required anchoring length. The frame was subjected to two phases of cyclic loading. In the first loading phase, the frame was subjected to the cyclic loading protocol shown in Fig. 7a. Due to test limitations, the maximum displacement in the push and pull directions was 75 mm. At the beginning of loading, complete fully reversed cycles were introduced, and then three fully reversed cycles were considered at each drift. To go beyond the 75 mm displacement, a second phase of loading was conducted in the push direction only with the loading protocol shown in Fig. 7b. The same loading protocol was utilized in the FEM for calibration. To control the computational time, the repeated cycles at each drift ratio were ignored. Considering that the three cycles in the experimental test produced almost identical responses due to the elastic properties of GFRP, the first cycle at a new drift level often produces the most significant changes in structural response (e.g., cracking, strains, etc.). A similar approach has been previously adopted in numerical simulations of GFRP-RC elements under cyclic loads to reduce computational time while achieving acceptable results in terms of load-hysteresis behaviour and failure modes [39,40]. Hence, only the first cycle of each drift was considered. The introduced load protocol to the model is shown in Fig. 7c.

A comparison between the hysteresis behaviour from the experiment and the FEM in the two phases is shown in Fig. 8. The results demonstrate good agreement between the test results and the model results. In the first loading phase, the response in both push and pull directions from the model was approximately symmetric, which aligns well with the test results despite minor discrepancies between the push and pull directions in the test results with different measured drifts at the last cycle. Such discrepancies are acceptable, considering that the machine had reached its maximum drift amplitude in the test. The model was also able to capture the self-centring behaviour of the frame due to the linear elastic behaviour of GFRP, as well as the length of pinching, which refers to the localized region of the hysteresis response where stiffness degradation and narrowing of the hysteresis loops being observed during unloading and reloading. In the second loading phase, the model also captured the response of the frame effectively. Due to the effect of the first loading phase, the stiffness of the frame in the second loading phase dropped, and the response was approximately linear, which is well captured in the model results.

The envelope load drift curves are shown in Fig. 8. The results indicate that both test results and model results exhibit almost the same response. The peak load obtained from the test was 107 kN, while the peak load obtained from the finite element model was 106 kN. The model was also able to capture the stiffness variation in both the first loading phase and the second loading phase. In terms of cracking patterns and failure mode, the model's results showed a similar failure mode to the experimental results. Major cracks were observed at the ends of the columns while beam cracks were localized around the connection region and especially at the clamping points. As shown in Fig. 9, both model and test results showed similar crack and failure patterns in the beam and column. As shown in Fig. 9, the ends of the right and left columns in both test and model results suffered severe damage. Also, the crack developed in the beam were also accurately captured in the model.

For further investigating the accuracy of the finite element model, the strains in the connection reinforcement at the top and bottom connections were obtained and analysed in comparison to the experimental test results. As shown in Fig. 10, the model aligns closely with the test results. The model effectively captures the significant difference in the maximum positive and negative directions and accurately reflects the strain differences between the top and bottom connections. For the maximum strain values, the difference between the model and the experimental results was 3 % and 9 % at the top and bottom connection, respectively. Despite the acceptable level of accuracy in the predicted strains, some discrepancies were observed at different drift ratios. These differences can be attributed to slight variations in the theoretical position of the strain gauges during testing, particularly in this sensitive

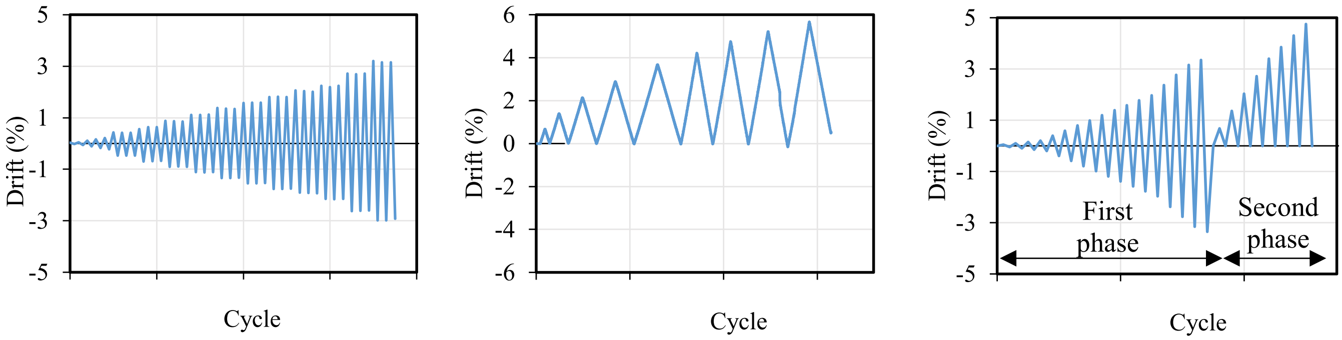

(a) Phase one protocol (b) Phase two protocol (c) Combined protocol

Fig. 7. Cyclic load protocol [32].

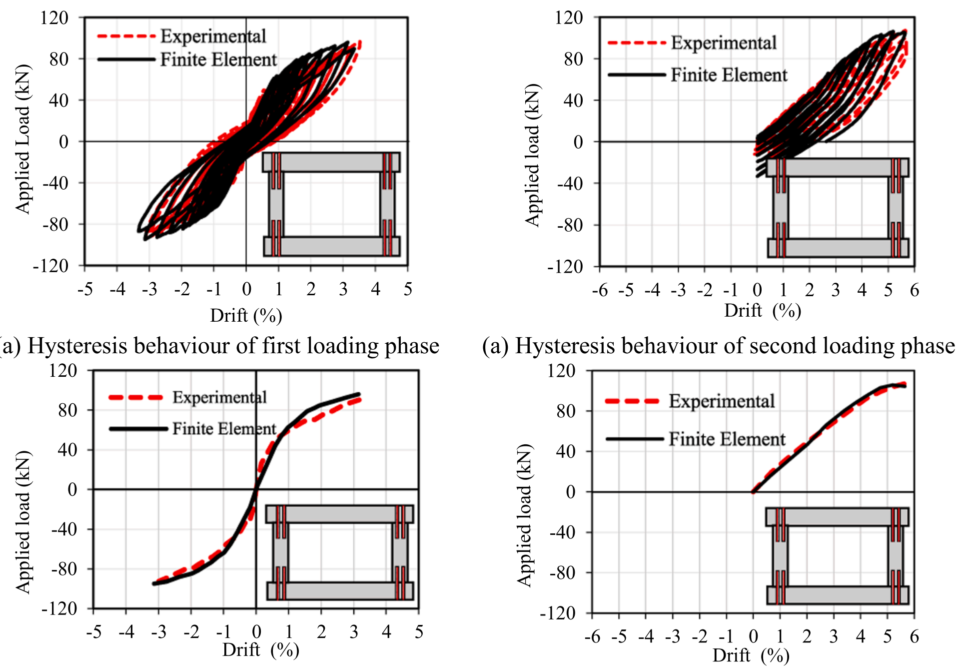

(a) Hysteresis behaviour of first loading phase (a) Hysteresis behaviour of second loading phase

(c) Load-drift envelope of first loading phase (d) Load-drift envelope of second loading phase

Fig. 8. Comparison between test and model results [32].

region of high strain concentrations. Overall, the results, including hysteresis behaviour, failure modes, and strain distribution, demonstrate the capability of the developed model to accurately simulate the cyclic performance of the investigated precast GFRP-RC frame.

4. Parametric study

The validated model was utilized to examine the impact of various parameters. Multiple FEA models were then developed to assess the effect of connection reinforcement material using connection bars. This included the comparison with cast-in-place frames, as well as investigating the influence of connection location and changes in section failure control. Finally, the results were juxtaposed with those of steel-RC counterpart frames. It is important to note that due to steel yielding, the second loading phase cannot be applied to model steel-RC structures owing to permanent deformations. Furthermore, since FEA can mitigate test limitations, the loading protocol was updated to consist of only one phase with increased drift ratios, as shown in Fig. 11.

The parametric study matrix is listed in Table 4. The examined frames were named to reflect the type of reinforcement, connection location, the material of connection reinforcement, and section failure control. The first letter denotes the reinforcement material for the precast beam and column, where "G" indicates GFRP, and "S" indicates steel reinforcement. The subsequent number describes the location of the connection, where the number "1" indicates the prefabricated ducts located in both column and beam, the number "2" indicates ducts located in the column only, and number "3" indicates ducts located in the beam only. The letters "R" or "C" replacing the numbers indicate whether the reference frame is subjected to the test loading protocol, or it is a cast-in-place frame, respectively. The letters following the dash indicate the material of connection reinforcement, where "G" is GFRP, "C" is Carbon Fiber Reinforced Polymer (CFRP), "MS" is mild stainless steel, "HS" is high-strength stainless steel, and "S" is reinforcement steel. Finally, the star symbol "* " indicates a compression control failure instead of tension control.

4.1. Effect of changing the loading protocol

The updated loading protocol enables reaching applied displacement up to 90 mm, corresponding to a drift ratio of 4.1 %, with a reduced

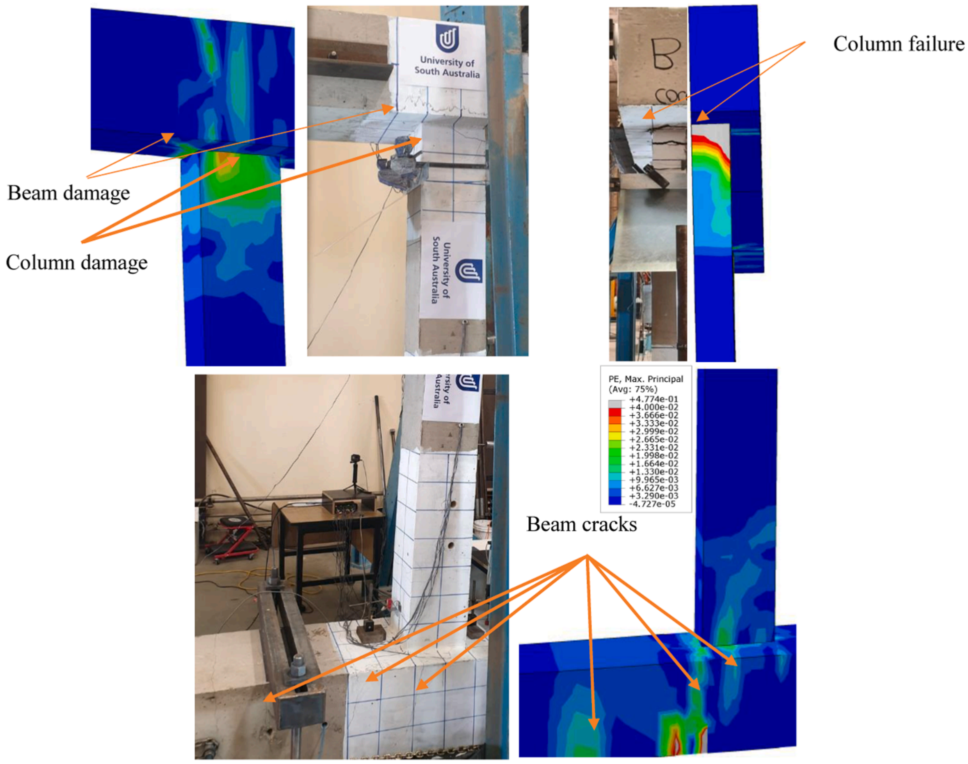

Fig. 9. Comparison between frame failure from test and model [32].

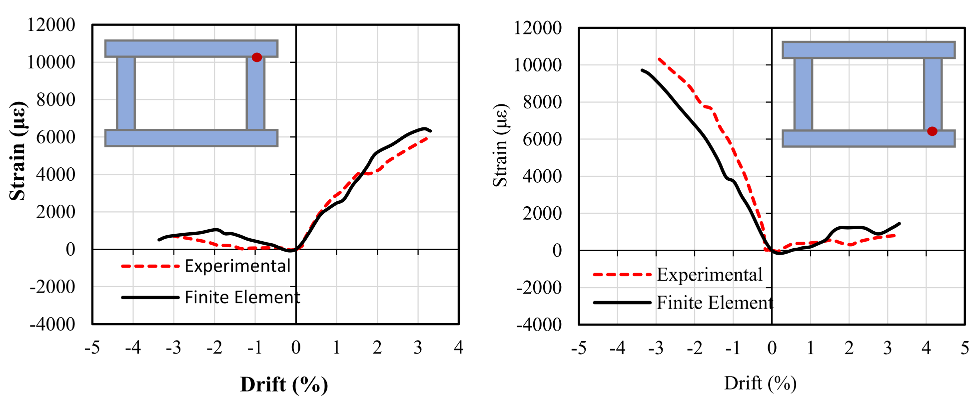

(a) Top connection (b) Bottom connection

Fig. 10. Comparison between strains in the connection reinforcement from test and model [32].

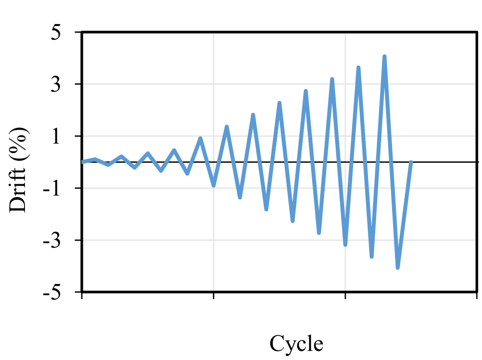

Fig. 11. Updated cyclic load protocol.

number of cycles to save both disk space and running time. The maximum applied drift was set to 4.1 %. Although different international codes specify a maximum lateral drift ratio of 2.5 % to prevent structural instability caused by excessive P-Δ effects and avoid damage to non-structural elements [41–43], the Canadian standards for the design of GFRP-RC structures CSA [44] adopted a maximum lateral drift ratio of 4 %. Additionally, the majority of experimental studies on GFRP-RC connections found that the capacity is almost attained at 4 % drift and found that this limit is suitable to be considered as a reference point to evaluate the cyclic behaviour [17]. Therefore, the ratio of 4.1 % was considered to evaluate the cyclic behaviour from a practical point of view that allows for studying the structural behaviour within a reasonable range, as such levels of drift may occur in extreme seismic events or unique design cases. The results under the test loading protocol and updated loading protocol were compared as shown in Fig. 12. The figure illustrates the previously obtained hysteresis response in the first loading stage and the hysteresis response under the updated loading

Table 4
Parametric study matrix.

Investigation	Frame	Description
Drift amplitude	GR-G	Reference
	G1-G	Increased drift amplitude
Material of connection reinforcement	G1-C	Carbon fibre-reinforced polymer
	G1-MS	Mild stainless steel
	G1-HS	High-strength stainless steel
Connection details	GC	Cast in place
	G2-G	Precast connection in column
	G3-G	Precast connection in the beam
Section failure control	GC*	Cast in place-compression control failure
	G1-G*	Precast connection in beam and column-compression control failure
	G2-G*	Precast connection in column-compression control failure
	G3-G*	Precast connection in the beam-compression control failure
Steel reinforced counterparts	SC	Cast in place
	S1-S	Precast connection in beam and column
	S2-S	Precast connection in column
	S3-S	Precast connection in the beam

protocol. In both cases, similar behaviour was observed in terms of stiffness, peak load, and overall load-drift envelope. The different loading protocols had only slight effects on the load-drift behaviour of the frame. The observed differences in Fig. 12, particularly in the hysteresis behaviour, can be attributed to the inclusion of multiple small drift cycles in the original load protocol, which caused the hysteresis loops to intersect. In contrast, the updated load protocol eliminates these small drifts, resulting in a clearer visualization of each loop. However, when considering the envelope curve shown in Fig. 12c, the behaviour remains largely consistent. A slight variation was observed at the peak drift of the test loading protocol because the drift did not coincide with the original drift value. The updated loading protocol demonstrates the advantages of studying the post-peak behaviour, which can be utilized to conduct further parametric studies, particularly in comparison with steel-reinforced counterparts.

4.2. *Effect of connection reinforcement material*

The influence of using connection reinforcement with different materials on the cyclic behaviour of the frame was evaluated. In addition to the reference connection material using GFRP, the use of CFRP, high-strength stainless steel, and mild stainless steel was considered. All considered reinforcement options have the same diameter as in the reference frame to enable direct comparison. The chosen reinforcement material has high corrosion resistance to be consistent with the reinforced used in the precast elements for the harsh environments. Table 5 shows the mechanical properties of the different materials. As listed in Table 5, GFRP has the lowest modulus of elasticity among the various options. CFRP was considered to study the effect of the modulus of elasticity on the cyclic behaviour, despite the similar linear elastic behaviour of GFRP and CFRP. Two types of stainless steel (high-strength and mild) were considered to study the effect of early and late yielding on the hysteresis behaviour of the frame, particularly in terms of widening hysteresis loops and enhancing energy dissipation capacity.

Fig. 13 shows the hysteresis response of the frame with the four connection reinforcement options. The results demonstrate significant differences in the hysteresis behaviour. No bar rupture was observed when GFRP or CFRP was used as connection reinforcement because of its high tensile strength. Due to the higher modulus of elasticity for CFRP than GFRP, both the peak load and initial stiffness were higher. This enhanced stiffness resulted in a higher peak load at an earlier drift of 2.7 % compared to 3.2 % in the case of using GFRP reinforcement. Additionally, the hysteresis loops became wider with the use of CFRP. This can be because of the improved rigidity of the connection that led to higher capacity and subsequently better contribution of inelastic deformations of concrete. The frame with high-strength stainless steel reinforcement (HS) exhibited similar hysteresis behaviour to that with CFRP reinforcement. However, the load was peaked at a drift of 2.2 % for HS, while peaked at a drift of 2.7 % for CFRP due to the higher modulus of elasticity for stainless steel than CFRP. Significant differences were identified between the performance of frames with HS and mild stainless-steel reinforcement (MS). The low yield stress of MS led to a reduced capacity compared to the frame with HS, and the maximum load was obtained at a drift ratio of 0.9 %. Despite the reduced capacity of the frame with MS, the permanent deformations due to reinforcement yielding led to widening the hysteresis loops and achieved a stable response up to a drift ratio of 4.1 %.

The failure mode of the four frames is shown in Fig. 14. Main damage was observed at the end of columns in all frames with less critical cracks in the beams. The cracks at the lower beam were more severe than those formed at the upper beams because of the stress concentration at the clamping points. Since frame G1-MS exhibited the least load-carrying capacity due to the earlier yield of the connection reinforcement (see

Table 5
Properties of different materials for connection reinforcement.

Material	Modules of Elasticity (MPa)	Yield stress (MPa)	Ultimate strength (MPa)	Reference
GFRP	60500	-	1200	[32]
CFRP	158000	-	1758	[45]
HS	200000	589	830	[46]
MS	200000	230	510	[47]

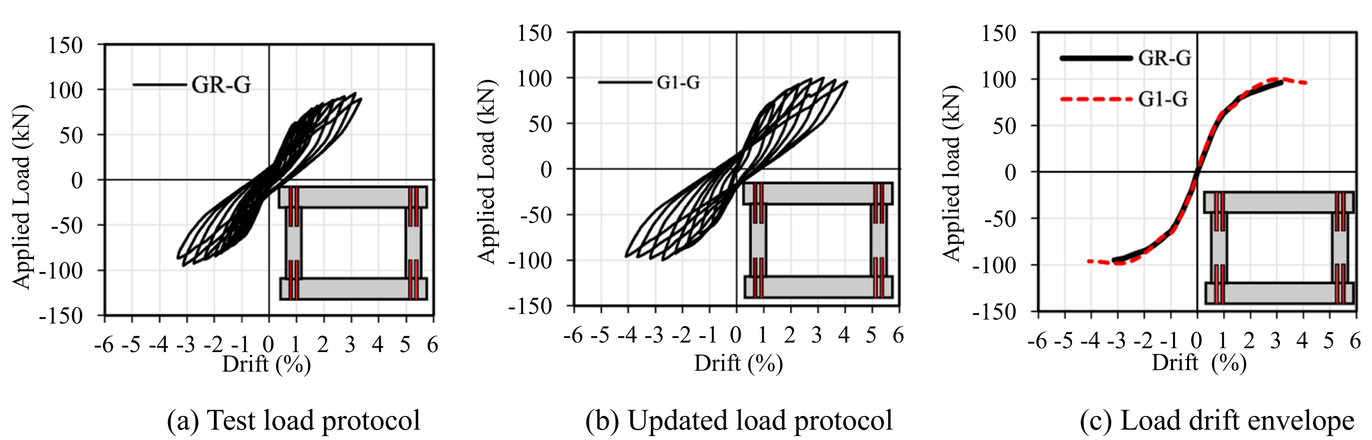

Fig. 12. Results with different cyclic load protocol.

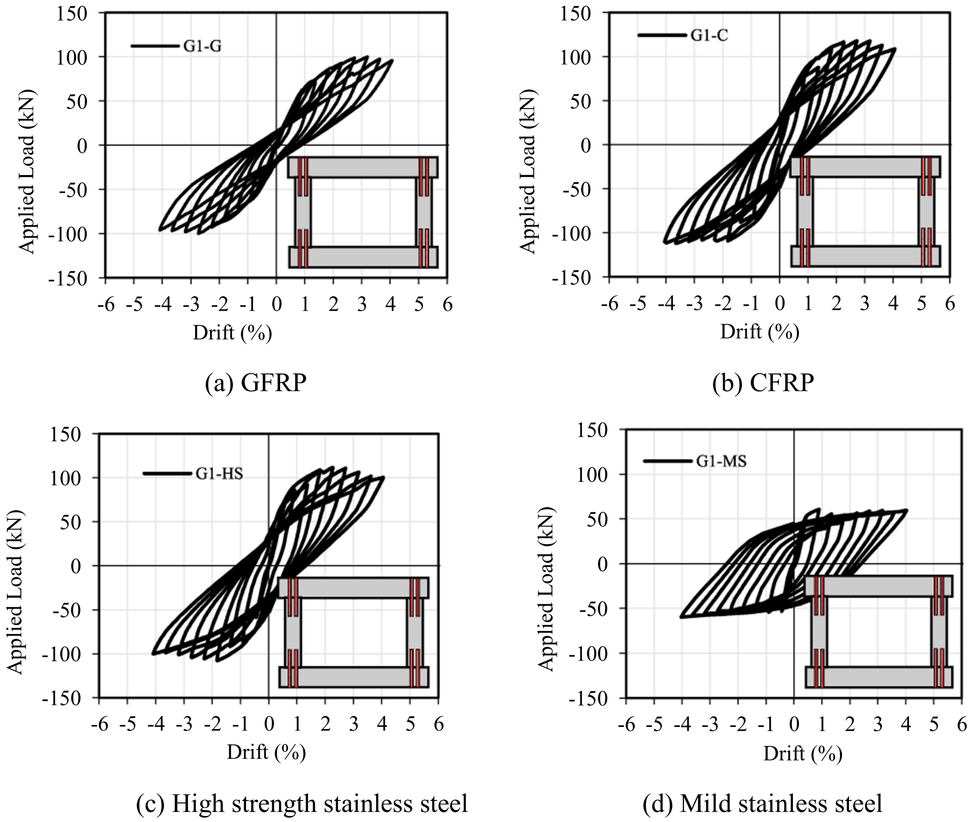

Fig. 13. Hysteresis behaviour of frame with different connection reinforcement.

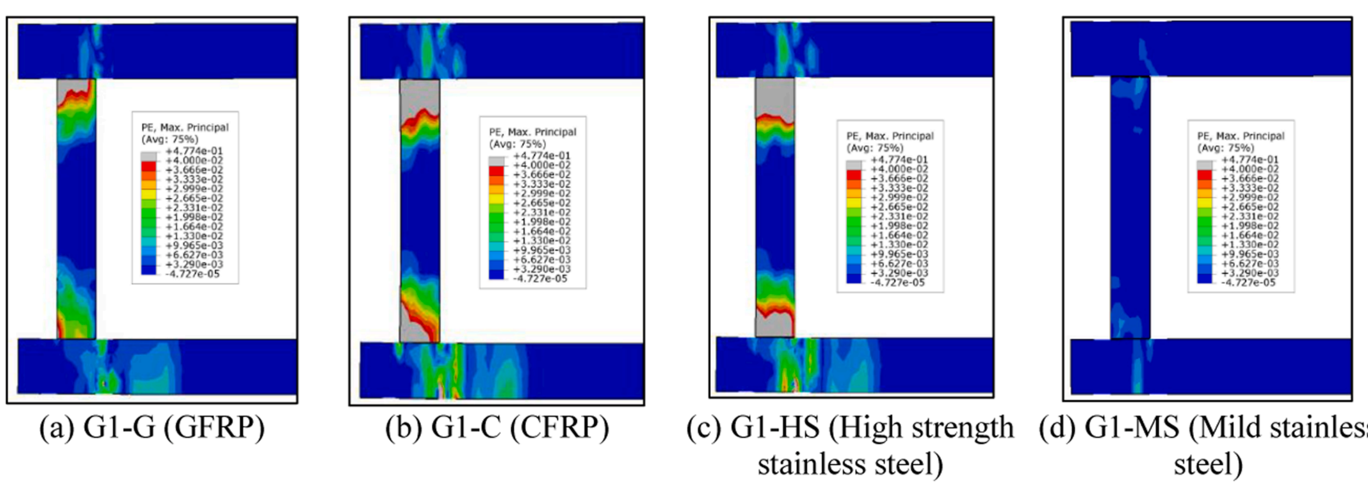

Fig. 14. Failure of frame with different connection reinforcement.

Fig. 15a), it suffered the least cracks. Meanwhile, the length of the damaged region of the column in frames G1-HS and G1-C was greater than that in G1-G due to higher load capacity led to introducing higher forces in the connection reinforcement. The earlier yield of the dowels in frame G1-MS led to a different crack formation and propagation mechanism as the yielding occurred very early resulting in reduced load-carrying capacity of the connection. Once the dowels yielded, the connection experienced stress redistribution, where the load was less efficiently transferred to the concrete. This reduced the development of additional stresses in the surrounding concrete and, consequently, limited the extent and severity of cracking. Additionally, the strain development in each frame was significantly different. The strains of frames with stainless steel reinforcement showed a sudden increase after yielding. As expected, the connection reinforcement of frame G1-MS yielded at an earlier drift ratio compared to G1-HS. The yielding of connection reinforcement in G1-HS at delayed drift enables higher forces to be developed in the connection reinforcement before yielding takes place. This explains the quite similar capacity obtained in G1-C and G1-HS where the failure became governed by slippage and splitting cracks around the ducts due to high forces, hence, the failure mode was similar to that of G1-C. This led to the presence of permanent deformations in a damaged region with significant slippage thereby, permanent deformation did not affect the frame response. Fig. 15a also shows that the strains in GFRP and CFRP in frames G1-G and G1-C are significantly less than their rapture limit frames with a gradual increase in the strains indicating that no rupture failure occurred. This is in line

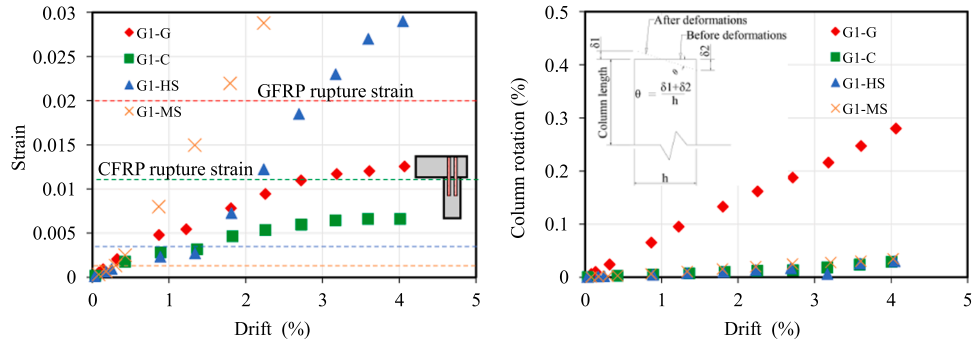

(a) Strain of connection reinforcement (b) Column rotation

Fig. 15. Reinforcement strains and column rotation with different connection reinforcement materials.

with the observation in the experimental study of the GFRP-RC frame.

Column rotation was analysed to evaluate the rigidity of the connection, which is the column deformation at the extreme points at each point of the column face divided by the thickness of the column cross-section. As shown in Fig. 15b, the frame G1-G exhibited the largest column rotation indicating higher deformation of the column and confirming the less rigidity of connection due to reduced modulus of elasticity of GFRP. Significant control of column rotation was observed in frames G1-C, G1-HS, and G1-MS due to fewer deformations attributed to higher modulus of elasticity of connection reinforcement for CFRP and stainless steel. This observation can explain the higher capacity of frame G1-C compared to G1-G.

The envelope load-drift curves are shown in Fig. 16a. At the beginning of loading, all frames exhibited linear elastic response. This is followed by nonlinear behaviour due to inelastic compression deformations of concrete and the yield of stainless steel until reaching the peak load. All frames showed a gradual degradation of strength in the post-peak behaviour. Despite the linear elastic behaviour of GFRP and CFRP, no sudden reduction of the strength was reported due to the absence of bar rupture. The capacity obtained using GFRP, CFRP, HS, and MS was 99.6 kN, 117.6 kN, 111.6 kN and 60.5 kN, respectively. The lateral capacity of frames using CFRP, HS, and MS was found to be 1.18, 1.12, and 0.61 of the capacity of the reference frame with GFRP reinforcement, respectively. The improvement of capacity by 18 % and 12 % in the case of using CFRP or HS, respectively is due to offering stiffer connection. Whereas, the reduction of capacity by 39 % in the case of using MS is attributed to the early yield of the MS.

The cyclic performance is evaluated through three indexes, namely residual drift, energy dissipation, and stiffness deterioration. Residual drift is an important index that reflects the functionality of the structure after repeated loads. The energy dissipation capacity indicates the ability of the structure to dissipate the input energy from the cyclic

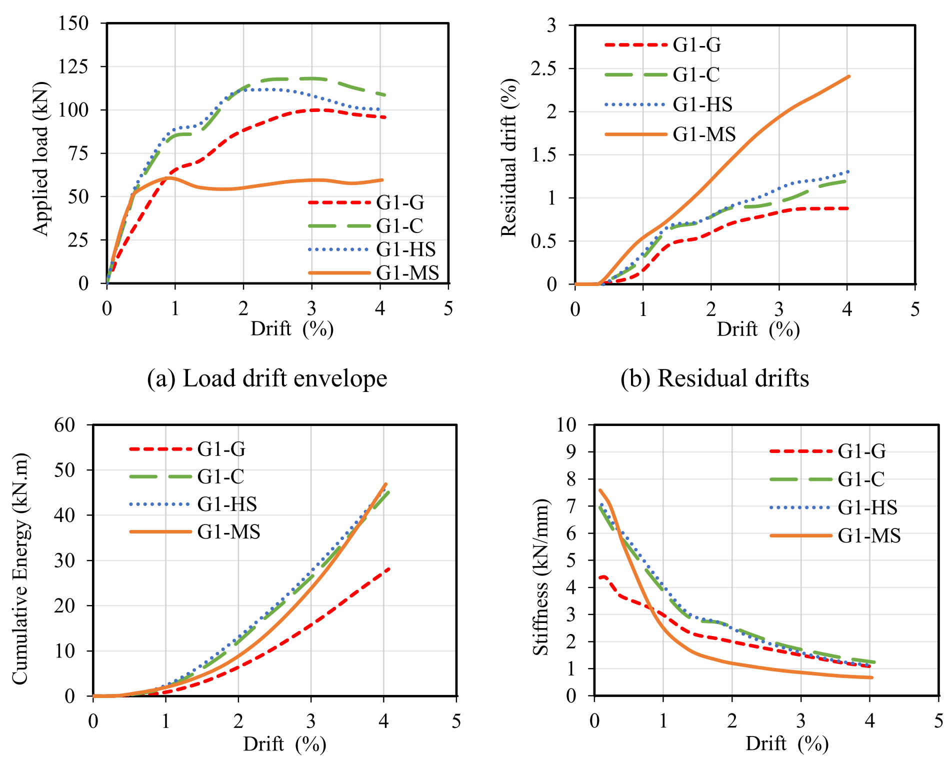

(a) Load drift envelope (b) Residual drifts

(c) Cumulative energy dissipation (d) Stiffness deterioration

Fig. 16. Cyclic performance evaluation of frame with different connection reinforcement materials.

loads. Under cyclic loads, the area of the hysteresis loops reflects the amount of energy dissipated in each cycle. The cumulative damage due to cyclic load can be reflected through stiffness deterioration. Stiffness is calculated for each cycle by considering the slope of the line passing through positive and negative peak points.

Fig. 16b shows the residual drift in the four cases of connection reinforcement. The results demonstrate that no residual drift is observed up to a drift ratio of 0.5 %, as the frames remained within its elastic range. Beyond this point, residual drift varies and increases with the applied drift, depending on the type of connection reinforcement. Frame G1-G exhibits the minimum residual drift, indicating its high self-centreing response. This reduced residual damage suggests that the structure returns to its original shape with minimal damage, requiring minimal repairs after cyclic loading. Both G1-C and G1-HS exhibited increased residual drift due to the enhanced inelastic contribution of concrete. The highest residual drift values exhibited by G1-MS reflect permanent deformations attributed to reinforcement yielding. While these higher residual drifts may pose challenges for structural repairs, they can be advantageous from an energy dissipation standpoint.

The cumulative energy dissipation is shown in Fig. 16c. Up to a drift ratio of 0.5 %, the energy dissipation capacity was negligible. The difference in the energy dissipation capacity among the considered options began to be noticeable at a drift ratio of 1.0 %. Beyond this point, a similar trend was observed in all four cases, where the cumulative energy dissipation increased with the drift ratio. At a drift value of 2.3 %, the cumulative energy dissipation of the frame G1-C, G1-HS, and G1-MS was higher than that in G1–1 by 80 %, 88 %, and 35 %, respectively. Although the capacity of frame G1-MS was only 61 % of that of G1-G, its energy dissipation was improved. This improvement can be attributed to the increased residual drift, which resulted in wider hysteresis loops after yielding resulting in an overall higher energy dissipation. At the drift ratio of 4.1 %, the energy dissipation capacity of the frame G1-C, G1-HS, and G1-MS was found to be 60 %, 66 %, and 67 % higher than that in G1-G, respectively.

Fig. 16d shows the stiffness deterioration of the frames with different connection reinforcement materials. As expected, the higher modulus of elasticity for CFRP, HS, and MS led to an improvement in the initial stiffness of the frame compared to the frame with GFRP. This improvement in initial stiffness was found to be 46 % in frame G1-C and reached 63 % in G1-MS compared to G1-G. Frames G1-G, G1-C, and G1-HS exhibited a lower rate of stiffness deterioration than those G1-MS. The rapid and increased rate of stiffness deterioration in G1-MS is due to plastic deformations caused by yielding, in addition to the other common sources observed in all four cases. These common sources of stiffness deterioration include concrete cracking, spalling, and the slippage of connection reinforcement. At the drift ratio of 4.1 %, all frames approximately had the same stiffness except for the frame with MS, which exhibited a final reduced stiffness.

4.3. Effect of connection details

The connection method in the reference frame was designed so that the connection reinforcement is assembled at the construction site. This connection method was referred to as (G1-G) as mentioned before. A comparison of the efficiency of this connection method with cast-in-place control frames and other common connection methods in the precast construction industry was evaluated. In this study, a model for a cast-in-place frame (GC) was developed, along with two other frames featuring different common connection methods (see Fig. 17). The frames were designed to investigate the effect of connection details. In addition to the reference connection in frame G1-G, where ducts exist in both the columns and beams, two common connection methods were considered: one involves using starter L-bars cast with the beam, passing into prefabricated ducts in the column (G2-G), and the other involves passing the column reinforcement through ducts prefabricated in the beam (G3-G), which are then filled with bonding material. Specimen G2-G was designed to have the same amount of connection reinforcement as in the reference specimen G1-G. The amount of connection reinforcement and the embedded length of bars in the column for frames G1-G and G2-G were the same. The primary difference in G2-G was that the reinforcement at the connection was cast with the cap beam as starter bars with sufficient anchoring length, leaving the ducts only in the column. This design enables an investigation into the behavioural differences and the contribution of the anchored length within the cap beam. Conversely, specimen G3-G represented a common conventional type of precast connection, where ducts were formed only in the cap beam. In this configuration, the connection reinforcement did not need to be precast with the column elements, as the extended column reinforcement served as the connection reinforcement. This design facilitates the study of the effects of having ducts only in the cap beams. In all cases, the same interaction method was applied by using epoxy resin for bonding, with the main difference being the connection reinforcement details.

Fig. 18 shows the hysteresis behaviour of the reference frame in comparison with the cast-in-place frame and the other two connection details. The results reveal significant differences in the hysteresis behaviour among the four cases. The initial stiffness, size of hysteresis loops, and pinching effect are strongly dependent on the connection details. While the peak load in frame G1-G was achieved at a drift ratio of 3.2 %, the peak load was reached at a higher drift ratio of 4.1 % in frame GC. In frame G2-G, the peak load was achieved at a drift ratio of 2.2 %. In the last frame G3-G, the peak load was reached at a drift ratio of 3.1 %. Although frame G1-G exhibited the least capacity among the examined frames, it shows a gradual strength reduction beyond the peak load. While frame G2-G showed higher capacity than G1-G, the results showed a higher reduction of strength beyond the peak load. The higher capacity is attributed to better anchoring of the starter bars with sufficient length inside the beam. Meanwhile, the frame G2-G exhibited reduced capacity compared to GC and G3-G due to the contribution of bar slippage at the column. On the other hand, both frames GC and G3-G did not show any strength reduction up to the maximum drift, and their response was quite similar. However, frame G3-G exhibited a sudden brittle failure due to increased stress at the interface between the column and beam causing the inability of the frame to continue due to bar

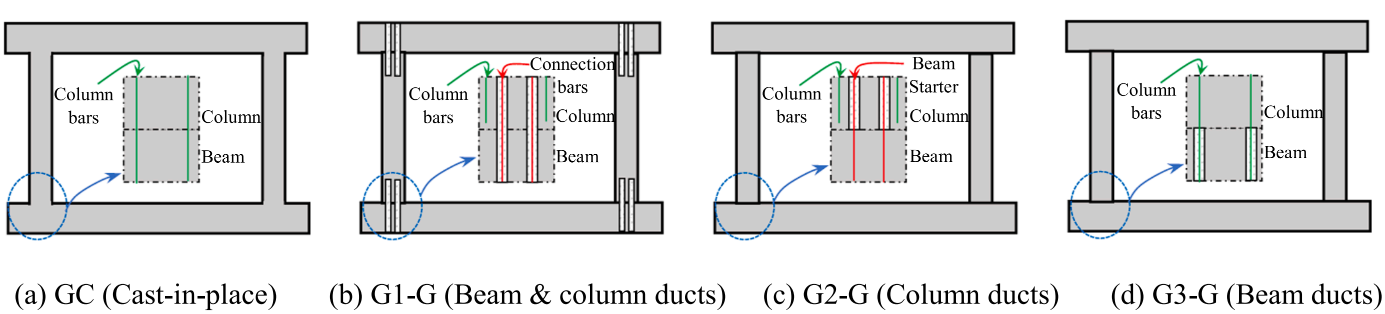

Fig. 17. Considered connection details of frame.

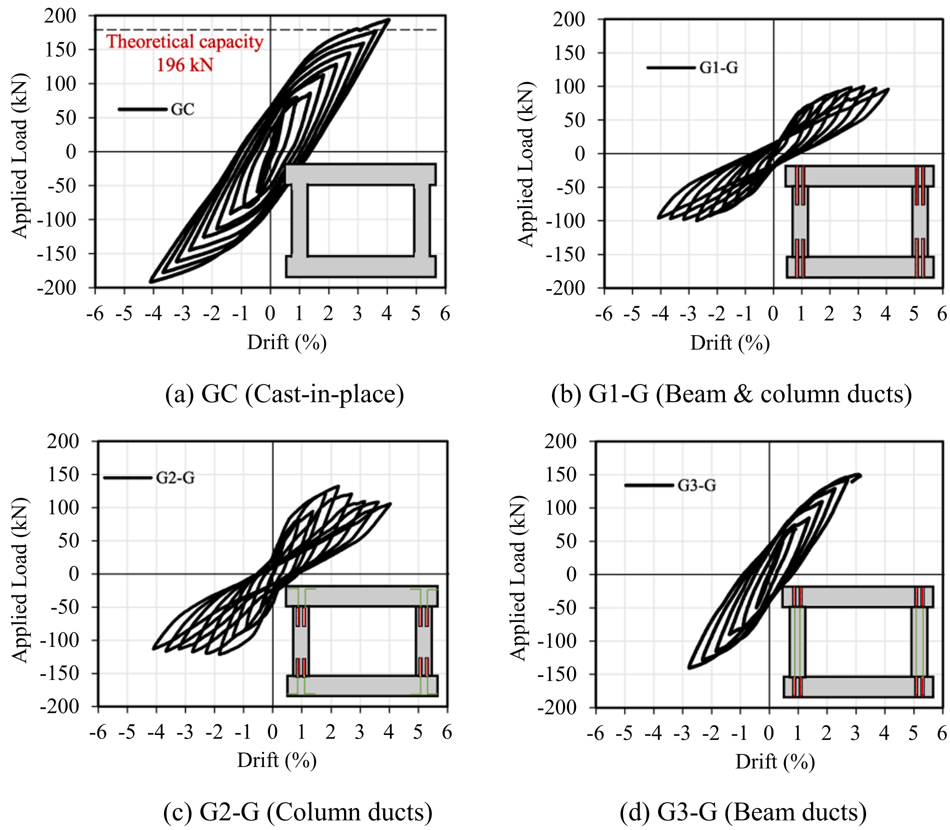

Fig. 18. Hysteresis behaviour of frame with different connection details.

rupture. The presence of the connecting ducts in the cap beam results in better performance and is recommended over placing them in the column due to better confinement to the ducts with larger volumes of concrete and ducts being away from the critical region in the column with most of the inelastic deformation occurred. This means that the column reinforcement should be sticking out from the precast column and only the connection with the cap beam be implanted using epoxy in situ.

The failure pattern of each frame is shown in Fig. 19. Each frame suffered a different crack pattern depending on the connection details. Frame GC suffered severe cracks at the connection due to higher introduced joint shear forces as well as greater rotation of the bottom beams. At the same time, the column suffered cracks at the plastic hinge region. However, the cracks were not as severe as those at the connection region at the beam since the column cross-section was designed to fail due to reinforcement rupture. Hence, the concrete of the column was not severely damaged. On the other hand, both frames G1-G and G2-G suffered severe damage at the column ends due to excessive damage around the unconfined ducts caused by the higher stress concentration and severe splitting cracks as well as slippage. These sources of damage when combined with the flexural cracks led to a significant damage and a reduced efficiency of these connection details. Unlike those two frames, the severe damage at the column ends was mitigated due to the elimination of improperly confined ducts at the critical region of the columns in frame G3-G. The ducts in this case are confined by a large volume of concrete within the beam. The crack pattern of G3-G was similar to that of GC; however, the cracks were less severe than those in GC due to the lower load capacity.

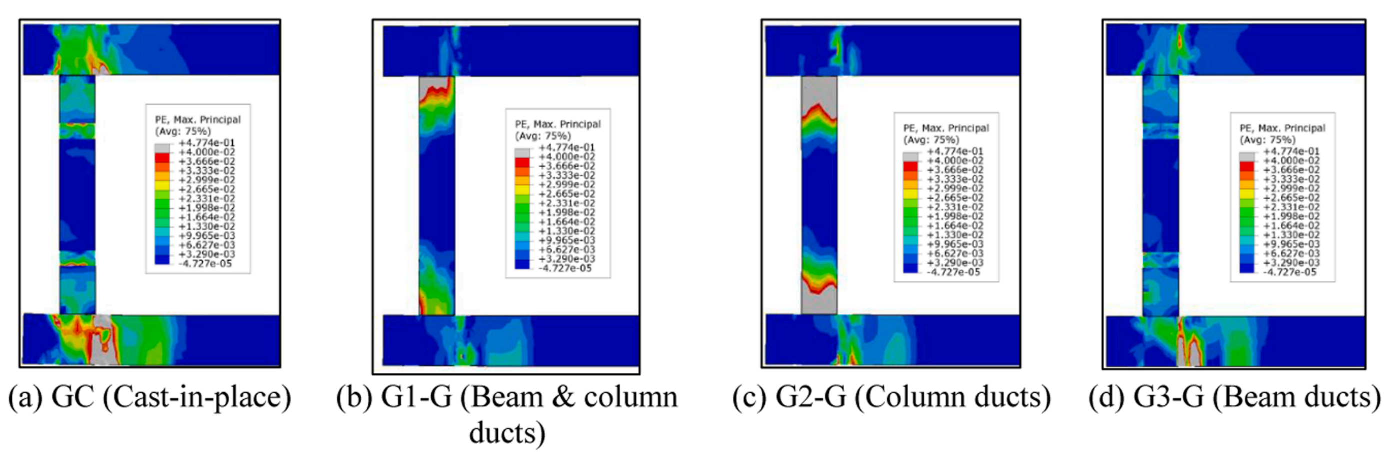

Fig. 19. Failure of frame with different connection details.

The strain of the reinforcement at the interface between the upper beam and column of the frames is shown in Fig. 20. The strain development depends on the connection details. At the same drift ratio, the reinforcement strains in frames GC and G3-G are higher compared to the other frames, aligning well with their greater load capacities. However, the results indicate that the reinforcement strains in frame GC are slightly below the rupture strain (0.02) of the bars. This is in good agreement with the theoretical calculation of the flexural capacity of the column section, which was designed to have tension-controlled failure. An increase in the applied drift ratio more than the considered drift is expected to result in a sudden drop in strength due to reaching the bars' rupture strains. Both frames GC and G3-G had similar values of the strains up to a drift ratio of 1.4 %. Beyond this limit, frame G3-G exhibited a higher strain of reinforcement at the interface between the beam and column. This subsequently caused frame G3-G to fail due to reaching the bar rupture strains at a lower load compared to that of frame GC. The earlier rupture of the bars is due to stress concentration at the interface between the beam and column, which is a common phenomenon in precast connections [31].

Fig. 21a shows the envelope load drift response of the four frames. The peak load for frame GC was 194 kN, which is greater than the peak load of the reference frame G1-G by 96 %. Meanwhile, the peak loads for frames G2-G and G3-G were 132 kN and 150.1 kN, respectively. These capacities are also greater than that of the frame G1-G by 33 % and 52 %, respectively. The reduced capacity of the reference frame is attributed to two reasons. Firstly, according to [31], such connection details should be designed with an amount of reinforcement of 1.25 times the column capacity to account for the effect of joint opening. In the reference frame G1-G, the amount of reinforcement provided at the connection was estimated to have the same capacity as the column at the section located at the interface between the beam and column. Secondly, as reported in [31], the embedded length inside the column should be at least 25 times the bar diameter, which is also not satisfied here. These two reasons also contribute to the obtained capacity of frame G2-G. However, frame G2-G exhibited a capacity 33 % greater than G1-G due to preventing the contribution of bar slippage in the beam. The response of both GC and G3-G followed a similar trend; however, due to the sudden rupture of the bars, frame G3-G was not able to resist higher forces. The mitigation of bar rupture can improve this drawback, potentially enabling the frame to resist higher loads. The subsequent section will discuss and compare the behaviour of these four frames when the frame columns are designed to have compression-controlled failure.

The residual drift of frame GC is greater than that of the three precast frames due to the greater contribution of inelastic concrete deformations resulting from the higher load introduced (see Fig. 21b). The energy dissipation of the four frames was almost the same up to a drift ratio of 1 %. Beyond this limit, the cumulative energy dissipation depended on the connection details. Both frames G2-G and G3-G dissipated energy

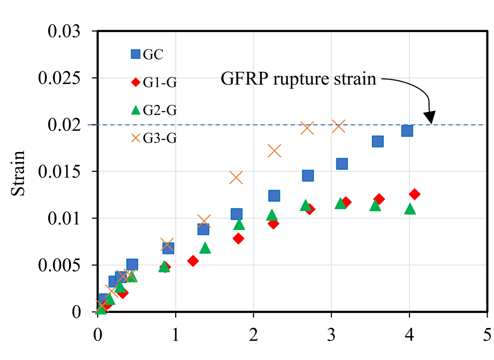

Fig. 20. Reinforcement strains at the connection interface for frames with different connection details.

77 % higher than that of G1-G at a drift ratio of 2.7 %. Despite G3-G dissipating 13 % higher capacity at 2.7 % drift compared to G2-G, the overall energy dissipation of G2-G was higher due to the brittle failure of the bars in G3-G. Fig. 21c shows that all precast frames dissipated significantly less energy compared to the cast-in-place counterpart (GC). This difference can be attributed to the less satisfactory cyclic behaviour of the precast frames, characterized by narrower hysteresis loops, reduced load-carrying capacity, and lower stiffness, which resulted in smaller loop areas. The rigidity of the connection also controls the initial stiffness of the frames. Due to no joint opening in the cast-in-place frame and no epoxy of low modulus of elasticity being used, the initial stiffness was higher than that of the precast frames. The G1-G frame had the lowest initial stiffness among the precast frames, primarily due to the epoxy-filled ducts in the beam and column (see Fig. 21d). Despite the higher initial stiffness of the GC frame, the rate of stiffness deterioration of GC was higher than that in frame G3-G at earlier loading stages. However, both GC and G3-G followed the same trend beyond a drift ratio of 1 %. As a result of bar slippage at the columns, both G1-G and G2-G continued to experience stiffness deterioration beyond a drift of 2 %. However, the deterioration is greater for G2-G, which agrees with the reduction of capacity beyond the peak.

4.4. Effect of changing the section failure control

The hysteresis behaviour of frames with the four details shown in Fig. 17 was restudied under different column reinforcement ratios. The balanced reinforcement amount was first determined. The process of determining the balanced reinforcement ratio for reinforced concrete structures with distributed tensile reinforcement may not be straightforward with a single formula and requires an iterative approach. The iterative process begins by inputting the necessary data, such as cross-sectional size, material properties, and reinforcement details. Initial values were set for the reinforcement area and neutral axis depth. The system then checks the force equilibrium and strain compatibility between the concrete and the reinforcement. If equilibrium is not achieved, the neutral axis depth is adjusted. If strain compatibility is not satisfied, the reinforcement area is modified. This process is repeated until both equilibrium and strain compatibility are met, allowing for the calculation and output of the balanced reinforcement amount. The process output indicated that the balanced reinforcement amount is 1144 mm^2. The reinforcement amount 8D13 (having a reinforcement area of 1061 mm^2) is below the balanced amount indicating a tension control failure. While 8D16 resulted in an amount of reinforcement of 1607 mm^2, exceeding the balanced amount, leading to compression control failure. The beam reinforcement, length of the longitudinal bars, as well as the properties of concrete and epoxy, were kept the same. As shown in Fig. 22, similar trends for each corresponding connection detail in the case of tension control failure were observed in the case of compression control design. However, the sudden failure due to bar rupture was mitigated, ensuring a more gradual failure mode. The results also demonstrated the closer response between frame GS* and frame G3-G*. Both frames G1-G* and G2-G* still experience lower capacities due to the combination of flexural cracks with splitting cracks around the unconfined ducts with the reinforcement slippage at the connection region since the embedded length inside the column was kept the same.

As shown in Fig. 23, the failure of the frames is quite similar to that shown previously in Fig. 19. However, due to changing the failure control from bar rupture to concrete crushing, the damage at the plastic hinge of the columns was more severe. The reinforcement strains at the connection interface shown in Fig. 24 confirm that all strain measurements in the four frames were below their rupture strain (0.02). The frames with ducts in the plastic hinge region of the column still suffered severe damage. Frame G3-G* failed in a way similar to the cast-in-place frame GC* despite the less critical cracks due to the 8 % reduction in capacity attributed to joint opening and slippage at the beam ducts. This

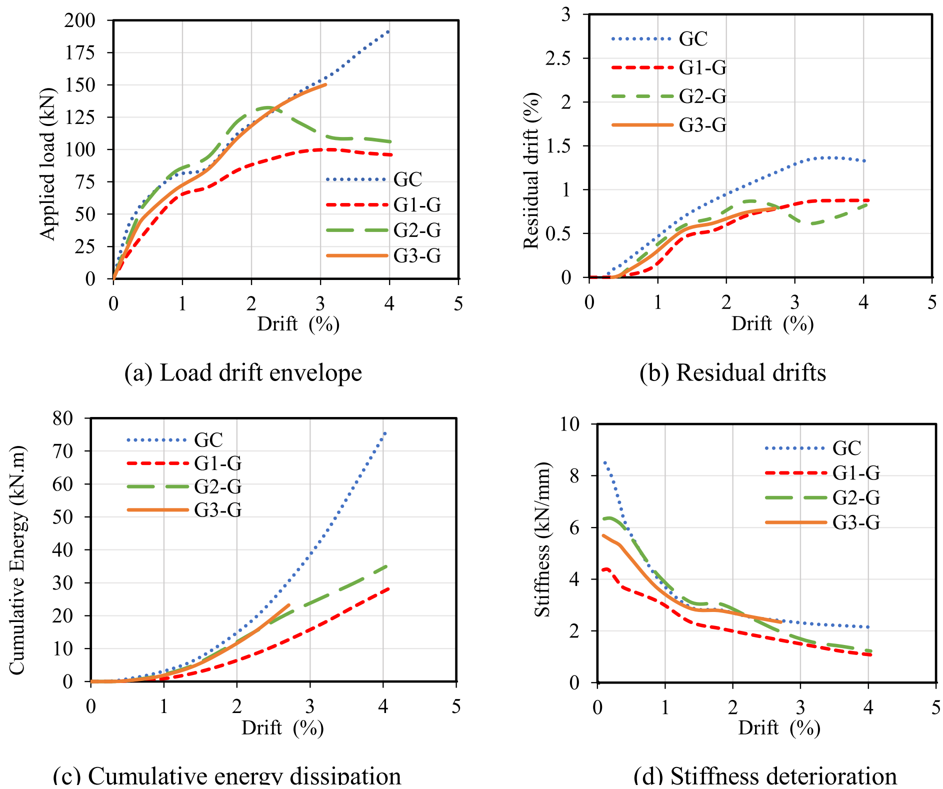

Fig. 21. Cyclic performance evaluation of frame with different connection reinforcement materials.

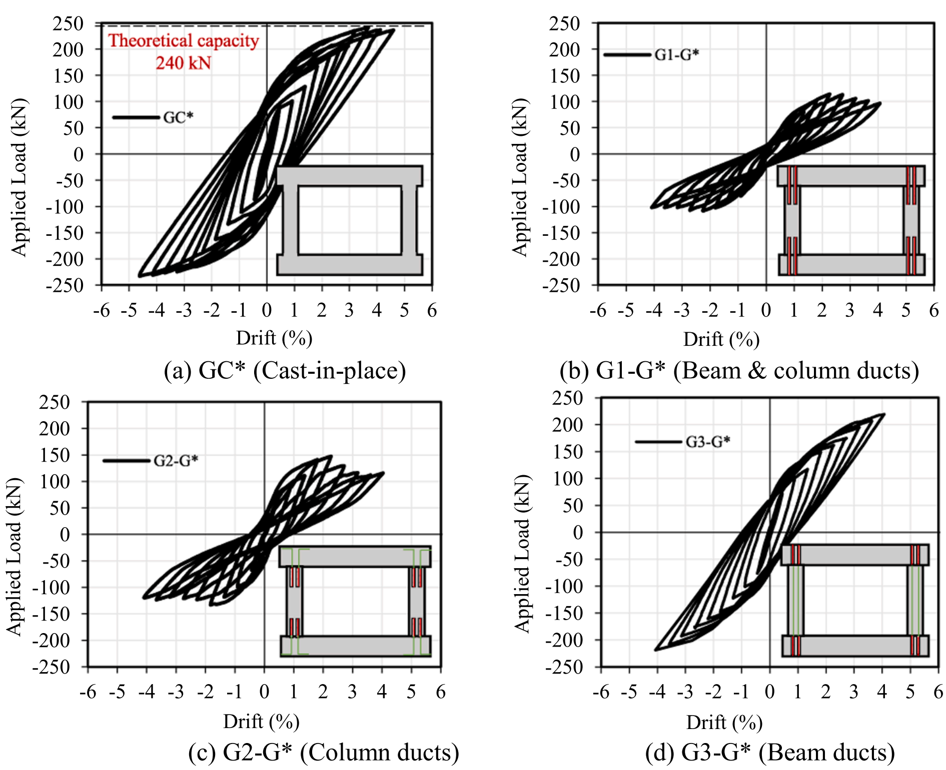

Fig. 22. Hysteresis behaviour of frame with different connection details - Case of compression failure control.

caused the concrete at the plastic hinge region of the column not to reach its crushing strain. This similarity of behaviour between GC* and G3-G* was also confirmed in the strain measurement of both frames (see Fig. 24). On the other hand, the maximum strain values in G1-G* and G2-G* were almost equal to those of G1-G and G2-G, which confirms that these frames experienced a local failure upon reaching the

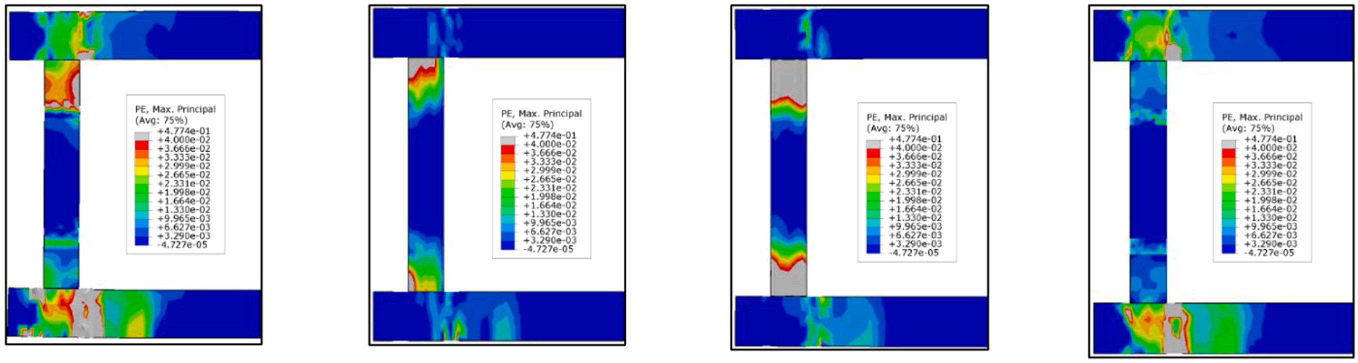

(a) GC* (Cast-in-place) (b) G1-G* (Beam & column ducts) (c) G2-G* (Column ducts) (d) G3-G* (Beam ducts)

Fig. 23. Failure of frame with different connection details - Compression control failure.

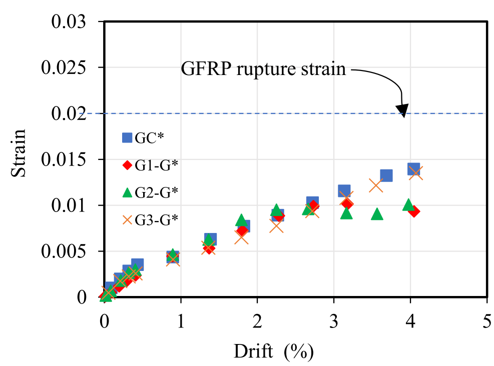

Fig. 24. Reinforcement strains at the connection interface for frames with different connection details- Case of Compression control failure.

maximum allowable concrete strength to resist splitting cracks and the forces necessary to induce slippage.

As shown in Fig. 25a, frame GC* reached its capacity of 241.8 kN at a drift ratio of 3.7 %, which is earlier than that obtained in GC with tension control failure as listed in Table 6. The increased reinforcement ratio of the column increased the capacity of the frame by 24 % and enhanced the stiffness, leading to achieving the capacity at an earlier drift ratio. Similarly, the increased reinforcement ratio in frame G1-G* increased the capacity from 99.8 kN to 132.4 kN (33 %). The increased amount of reinforcement increased the connection stiffness and led to achieving the maximum capacity at an earlier drift of 2.3 % compared to 3.2 % in G1-G with a lower column reinforcement ratio. Although there is an improvement in the capacity by 23 % for frame G2-G* compared to the counterpart frame G2-G, the post-peak trend is the same, where the frame still experiences a drop in capacity after achieving the maximum capacity. A significant difference in the behaviour of frames with a higher reinforcement ratio was observed for the frame G3-G* . The increased reinforcement ratio and mitigation of bar brittle failure significantly improved the structural performance. The capacity of frame G3-G* increased by 46 % compared to the counterpart frame G3-G. This increased ratio is due to the mitigation of reaching the ultimate strains of the reinforcement in compression control design even with considering the strain concentration phenomenon at the connection interface. While compared to the cast-in-place frame GC* , the difference in capacity was limited to 9 % due to the contribution of joint opening and the low modulus of elasticity of bonding epoxy. It should be noted that this difference was 23 % between G3-G and GC. It can be concluded that it is desirable to design the precast GFRP-RC frame with connecting ducts located at the beam and to ensure that the failure of the column section is governed by concrete compression rather than bar rupture under cyclic loads to mitigate the sudden catastrophic failure due to bar rapture at the connection interface.

As shown in Fig. 25, the differences in stiffness deterioration and energy dissipation among the four connection details are similar to the earlier reported results for frames with tension control failure. Frame GC* exhibited the highest initial stiffness and overall energy dissipation. However, both frames GC* and G3-G* exhibited the same value of stiffness beyond a drift ratio of about 0.5 %. Among the frames, GS* and G3-G* still have minimum deterioration of stiffness beyond a drift ratio of 1.5 %, while both G1-G* and G2-G* still experience stiffness deterioration up to the maximum drift ratio due to reinforcement slippage. Additionally, the energy dissipation capacity of frame G3-G* is the closest to the energy dissipation capacity of the cast-in-place frame GC* . As given in Table 6, the initial stiffness and energy dissipation capacity improved by increasing the column reinforcement ratio and changing the failure mode from bar rupture to concrete failure. Compared to the counterpart frames with tension control failure, a significant increase in initial stiffness by 75 % was found in frame G3-G* compared to G3-G. Due to changing the bar rupture failure mode of frame G3-G to concrete compression failure in frame G3-G* , the cumulative energy dissipation capacity was improved by 330 % due to the better contribution of concrete cracking and spalling in dissipating the energy. In terms of residual drift, the four frames exhibited lower values of residual drifts due to the elastic behaviour of GFPR reinforcement.

4.5. Comparison with steel reinforced counterparts frames

Four frames with the same four connection details in Fig. 17 were examined to evaluate the performance of GFRP-RC in comparison to conventional steel-RC frames. The steel-RC frames have the same reinforcement ratio as in the GFRP-RC with tension control failure. Concrete strength and epoxy properties were kept the same. The steel reinforcement used in these frames has a yield stress of 500 MPa as per the Australian standards AS4671 [48].

Fig. 26 shows the hysteresis behaviour of the four frames. As expected, the hysteresis behaviour was significantly different from that observed for GFRP-RC frames due to the inherent difference between steel and GFRP. Because of the high modulus of elasticity of steel reinforcement, the frames were able to reach their design capacity at earlier drifts. The yielding of steel reinforcement resulted in the residual drift and the size of hysteresis loops increased compared to those with GFRP-RC. It should be noted that all four steel-RC frames were able to reach their capacity, a difference from those with GFRP-RC, where the connection details had a significant impact on the achieved capacity. Because the forces in the connection reinforcement are limited by the yield stress, which is significantly less than the rupture stress of GFRP,

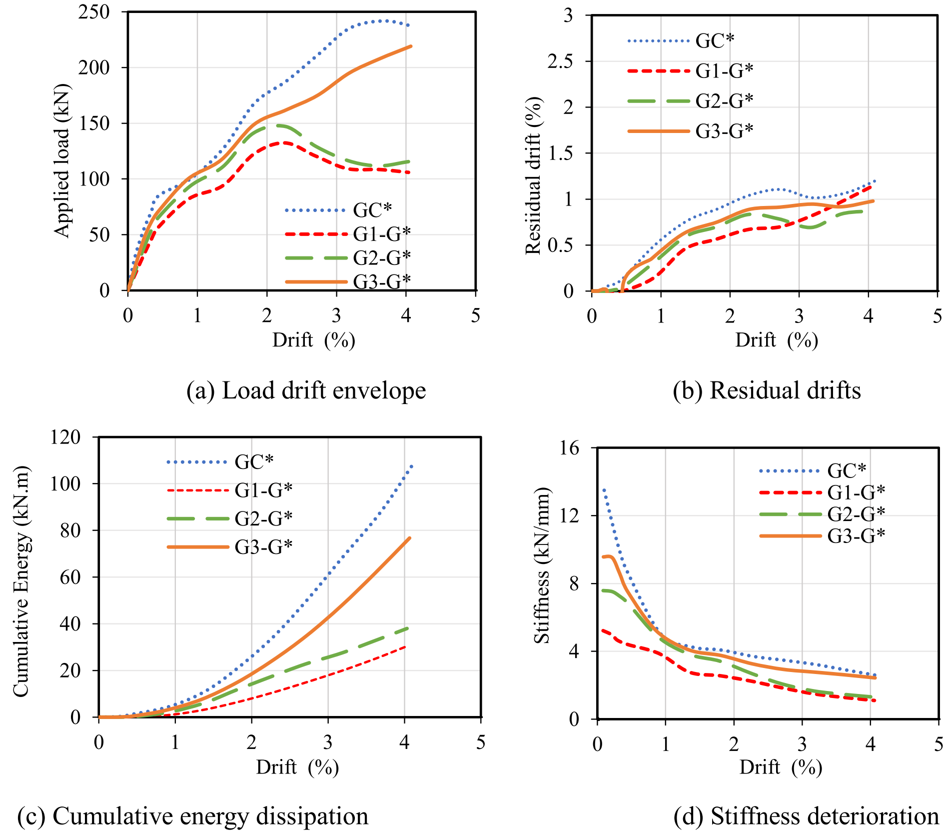

Fig. 25. Cyclic performance evaluation of frame with different connection reinforcement materials.

Table 6
Influence of section failure control on cyclic performance of GFRP-RC frames.

Frame		GC*	GC	G1-G*	G1-G	G2-G*	G2-G	G3-G*	G3-G
Influence on capacity	Capacity (kN)	241.8	194	132.4	99.8	161.7	132	219	150
	Corresponding drift (%)	3.7 %	4.1 %	2.3 %	3.2 %	2.3 %	2.2 %	4.1 %	3.1 %
	Capacity increased (%)	25 %		33 %		23 %		46 %	
Influence on initial stiffness	Initial stiffness (kN/mm)	13.5	9.5	5.2	4.4	7.6	6.4	9.6	5.5
	Improvement (%)	42 %		16 %		19 %		75 %	
Influence on energy dissipation	Overall cumulative energy dissipation (kN.m)	108.7	76.5	30.7	28.0	37.9	34.9	76.7	23.2
	Improvement (%)	42 %		9.5 %		8.9 %		330 %	
Influence on residual drift	Residual drift (%)	1.2	1.3	1.1	0.9	0.9	0.8	1.0	0.8
	Change (%)	8 %		22 %		13 %		25 %	

the effect of splitting cracks and slippage was less pronounced. Moreover, it is noteworthy that the presence of connection reinforcement in S1-S and S2-S led to achieving higher capacities than S3-S, as it added to the flexural capacity of the column, enabling the frame to reach its design capacity. However, the presence of column ducts reduced the residual drifts in frames S1-S and S2-S, while the hysteresis behaviour of S3-S was almost similar to the control cast-in-place frame SC.

The envelope load drift curves are shown in Fig. 27a. The predicted nominal lateral capacity of the columns is 105 kN. All frames achieved their design capacity. According to the results, frame SC reached a capacity of 123.8 kN at a drift ratio of 0.9 %. The precast frames reached their design capacities at different drifts, depending on the details of the connection. The frame S1-S reached a capacity of 116 kN at a drift ratio of 1.8 %. Whereas, frames S2-S and S3-S achieved capacities of 137 kN and 108.4 kN at a drift ratio of 0.9 %, respectively. Compared to frame SC, frame S2-S achieved a higher capacity by 11 % due to the benefits of starter bars in increasing the column flexural capacity. Although both GFRP-RC frames and steel-RC frames have the same amount of reinforcement, the steel-RC frames reached their capacities at drifts of less than 2.5 %, which is usually adopted in RC structures to control damage to non-structural elements, whereas, it was achieved at greater drifts than 2.5 % for GFRP-RC frames which is usally the case in GFRP-RC, as reported in [17]. However, according to [44], deformable GFRP-RC frames should be able to reach a drift ratio of 4 %.

The results in Fig. 27 followed similar trends to those observed with GFRP reinforcement regarding the effect of connection details on stiffness and energy dissipation capacities. Frame SC exhibited the greatest initial stiffness and overall energy dissipation. However, residual drifts became more significant in steel-RC frames due to the penetration of damage resulting from steel yielding, causing permanent deformations. At earlier drifts (less than 1 %), the amount of energy dissipation was negligible among different connection details. However, beyond this, energy dissipation increased due to steel yielding. Frame S3-S dissipated energy closer to the cast-in-place frame SC, owing to the large hysteresis loops, greater residual deformations, and yielding penetration into the cap beam. The two other frames, S1-S and S2-S, dissipated less energy

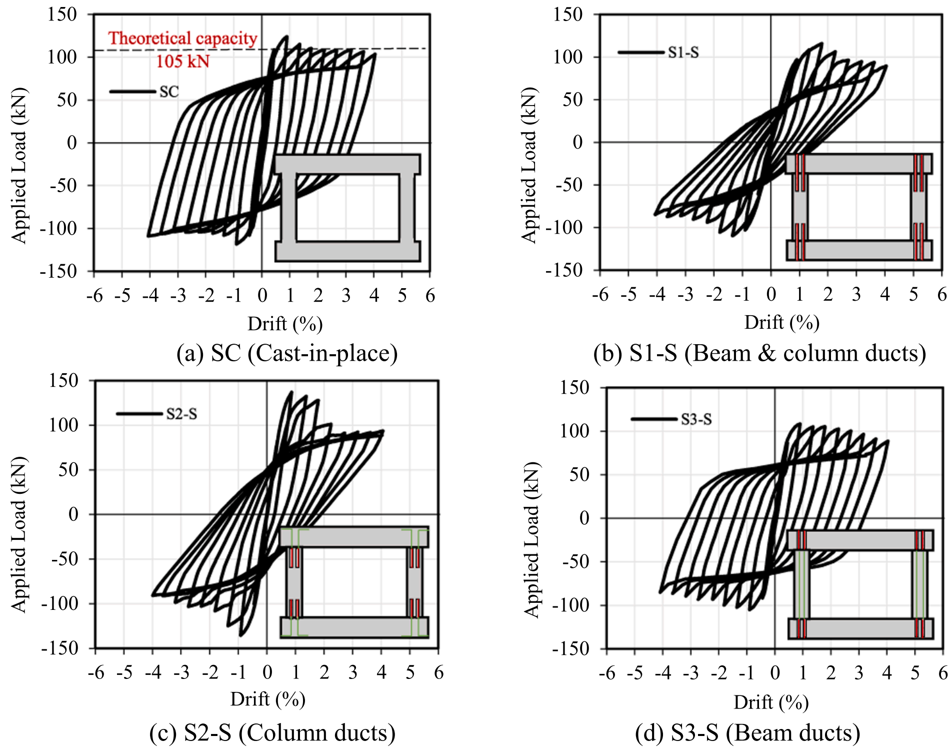

Fig. 26. Hysteresis behaviour of steel-RC frame with different connection details.

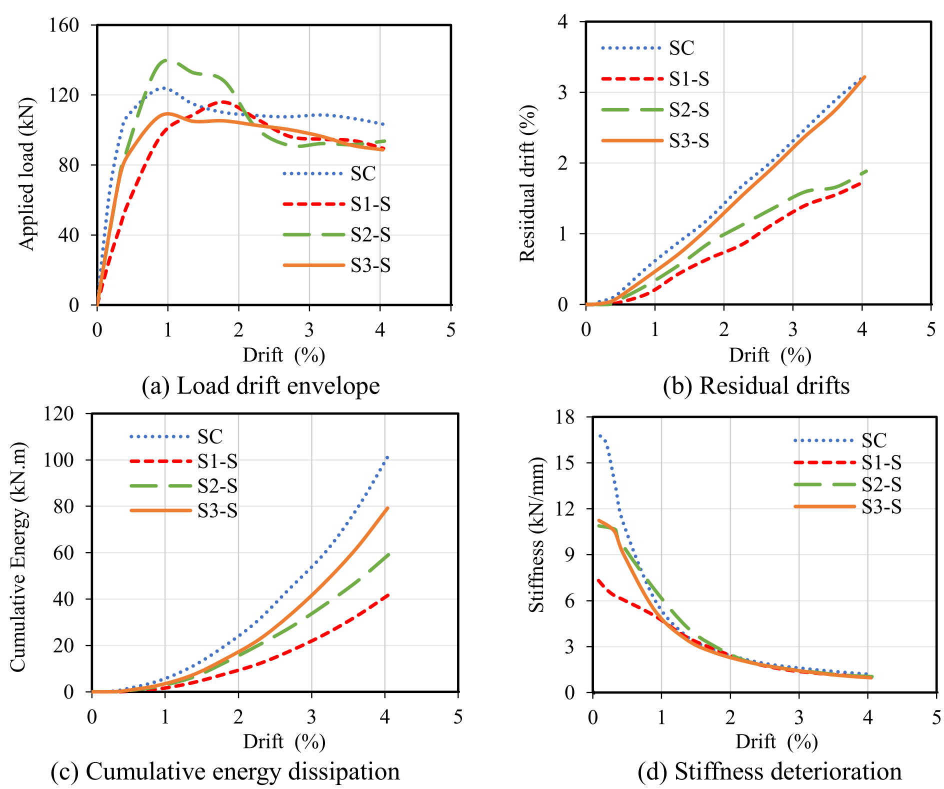

Fig. 27. Cyclic performance evaluation of frame with different connection reinforcement materials.

due to the smaller cyclic loop area, despite their higher capacities resulting from the presence of the connection ducts at the column end. In terms of stiffness deterioration, the rate of stiffness deterioration was quicker than that with GFRP, as a result of cumulative excessive damage. Unlike GFRP-RC frames, where the final stiffness depends on the connection details, the stiffness of all steel-RC frames became the same, since all frames failed due to the yielding of column reinforcement.

A performance comparison between the counterpart details of steel-

RC frames and GFRP-RC frames with tension and compression failure control was carried out. As shown in Fig. 28, the cast-in-place frames exhibited the greatest initial stiffness in the three cases, followed by precast frames with connections in the cap beam. In contrast, the precast frames with connections in both the column and beam achieved the least initial stiffness. However, due to the higher modulus of elasticity of steel, the steel-RC frames exhibited higher initial stiffness in all cases. Meanwhile, increasing the GFRP reinforcement ratio in the columns, which subsequently led to changing the failure from bar rupture to concrete compression failure, limited the gap between the initial stiffness of steel-RC and GFRP-RC frames, especially in the case of a connection in the cap beam. Although steel-RC frames exhibited the greatest initial stiffness, the final stiffness of steel-RC frames was the least in all cases. This can be explained by the excessive cumulative damage due to steel yielding causing significant stiffness deterioration. In conclusion, from a stiffness point of view, the precast GFRP-RC frame with a connection in the cap beam exhibited closer stiffness to the counterpart connection in the steel-RC frame, and at the same time, it exhibited the least stiffness deterioration among precast frames, approximately similar to the cast-in-place GFRP-RC frame.

The functionality of a structure after cyclic loads can be evaluated through residual drifts. The minimum residual drift indicates that the structure exhibits minimum damage and requires less repair. Fig. 29a shows significant differences between steel-RC and GFRP-RC frames. In general, all GFRP-RC frames exhibited significantly lower residual drifts compared to steel-RC frames. The minimum residual drifts are attributed to the linear elastic behaviour of the GFRP bars, which mitigate the permanent deformations in the structures, enabling the structures to return to their original condition and subsequently require minimum repair costs. On the other hand, steel yielding causes permanent deformations. However, frames with connections located at the column exhibited decreased residual drifts for steel-RC frames. In conclusion, while connection details can control the residual drift of steel-RC precast frames, GFRP-RC precast frames are advantageous in terms of residual drift compared to steel-RC frames regardless of the connection details.

A comparison between the energy dissipation capacities of the frames with GFRP and steel reinforcement is shown in Fig. 29b. Generally, all cast-in-place frames dissipated the highest amount of energy compared to the precast frames because of the stable hysteresis loops. Due to the different hysteresis responses between the cast-in-place steel-RC frame and GFRP-RC frame with the same amount of reinforcement, the steel-RC cast-in-place frame dissipated overall energy 33 % greater than the GFRP-RC frame. With an increase in the amount of GFRP reinforcement, the energy dissipation of the GFRP-RC frame was 7 % higher than the steel-RC cast-in-place frame because of the capacity increase as well as the better contribution of concrete in dissipating the energy. On the other hand, connection details in precast frames determine the ability of the structure to dissipate the energy regardless of the reinforcement type. In general, precast frames with epoxy-filled ducts located in both the column and beam dissipate the least amount of energy. Compared to the cast-in-place frame, the precast frame with epoxy-filled ducts located at the beam and the column dissipated less energy by 37 %, 28 %, and 41 % for the GFRP-RC frame with tension control failure, GFRP-RC frame with compression control failure, and steel-RC frame, respectively. Meanwhile, the precast frame with epoxy-filled ducts located at the beam dissipates 30 % and 22 % less than the cast-in-place frame reinforced with GFRP and steel, respectively. Despite this reduction in energy dissipation, the frame with epoxy-filled ducts located at the cap beam dissipates energy almost equal to the counterpart connection in the frame with steel reinforcement.

From the discussed results, it can be confirmed that a precast GFRP-RC frame with concrete compression control failure, designed with connecting epoxy-filled ducts located at the cap beam, can achieve superior performance in two different aspects. Firstly, the precast frame is comparable to an identical steel-RC frame with a typical connection in terms of initial stiffness and energy dissipation. However, it can outperform the steel-RC frame in terms of residual drifts and stiffness after loading, which can be more beneficial in terms of repairs. Secondly, the precast frame is capable of achieving acceptable performance compared to the reference cast-in-place frame with GFRP reinforcement.

5. Conclusions

The cyclic performance of precast GFRP-RC frames was investigated in this study. A finite element model (FEM) was developed and validated against a large-scale frame tested under cyclic load. Subsequently, the model was utilized to study the effect of different connection details. The effectiveness of the examined connections was also evaluated in comparison to equivalent cast-in-place models. Finally, a comparison was made between precast GFRP-RC frames and steel-RC frames, considering the connection details of each counterpart. The following conclusions can be drawn from the current study:

1. The hysteresis behaviour of the precast GFRP-RC frame assembled by dowels depends on the strength and stiffness of the material of connection reinforcement. With the same amount of reinforcement, CFRP or HS can achieve a capacity higher than that with GFRP by 18 % and 12 %, respectively due to their higher stiffness, while MS with low yield strength led to a reduction in capacity by 39 % compared to that with GFRP.
2. The cyclic performance, in terms of energy dissipation, stiffness deterioration, and residual damage, depends on the properties of the connection reinforcement material. Frames with connection reinforcement made of CFRP, HS, and MS dissipate significantly more energy and achieve greater initial stiffness than those with GFRP. Meanwhile, the frame with GFRP exhibited the minimum residual drift, whereas the frame with MS exhibited the maximum. Therefore, based on the design criteria, the connection reinforcement material can be selected to prioritize either energy dissipation or minimum residual damage.
3. Thelocation of epoxy-filled ducts significantly influences the performance of frames in terms of capacity, stiffness, and energy

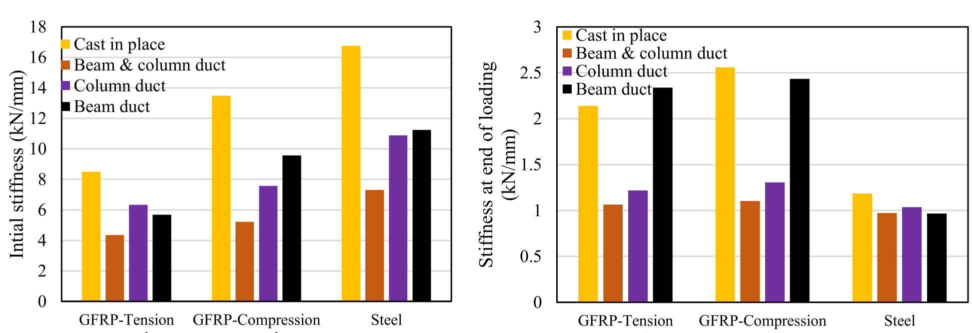

Fig. 28. Comparison between stiffness of GFRP-RC and steel-RC frames with different connection details.

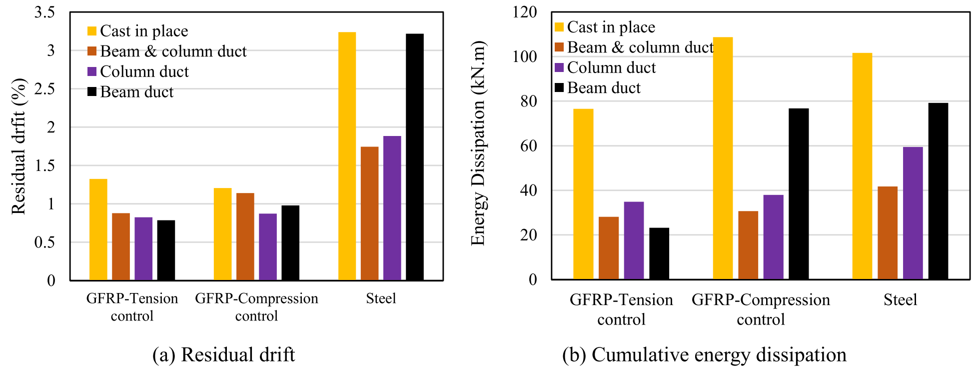

Fig. 29. Comparison between Residual drift and Cumulative energy dissipation of GFRP-RC and steel-RC frames with different connection details.

dissipation. The presence of the connecting ducts in the cap beam enhances the capacity by 65 % and 35 %, and the energy dissipation by 149 % and 102 %, compared to connections located in the columns and in both the columns and cap beams, respectively. This confirms that the embedded length in the column is more critical than that in the beam, where plastic hinges are formed and splitting cracks are severe around the unconfined ducts .

4. Failure of precast GFRP-RC frames is governed by the stress concentration at the interface between the beam and column. This stress concentration leads to reduced capacity due to either earlier bar rupture or bond degradation for the connection reinforcement depending on the location of the connecting ducts.
5. The optimum cyclic performance of GFRP-RC frames can be achieved by ensuring a concrete compression failure rather than bar rapture to avoid the risk of reaching earlier bar rapture at the interface in case of locating the connecting unconfined epoxy filled ducts at the beam.
6. In comparison to GFRP-RC frames with the same reinforcement ratio, steel-RC frames exhibited wider hysteresis loops and subsequently dissipated greater energy and achieved greater initial stiffness. However, GFRP-RC performed better in terms of residual drift and stiffness after loading.
7. A precast GFRP-RC frame can achieve comparable cyclic performance to that of a precast steel-RC frame and to the equivalent cast-in-place GFRP-RC frame by ensuring that the compression failure of concrete is the governing failure while designing the frame with connection epoxy-filled ducts located at the cap beam.

While the results reported in the current study provide a better understanding of the cyclic behaviour of precast frames with different connection details and propose a design philosophy for the optimum location of unconfined epoxy-filled ducts, there are some limitations due to the nature of the reference case study. The conclusions are specific to precast jetty frames assembled using epoxy resin, which failed due to the flexural failure of columns. Extending these conclusions to multistorey frames—where beams are typically weaker than columns and columns are extended on both sides of the beams, leading to beam flexural failure or other failure modes—requires further investigation. Future studies should also explore the effects of frame geometry, beam size, and beam length variations.

CRediT authorship contribution statement

Mohamed H. El-Naqeeb: Writing – original draft, Validation, Software, Methodology, Investigation, Formal analysis, Data curation, Conceptualization. **Reza Hassanli:** Writing – review & editing, Supervision, Project administration, Methodology, Funding acquisition, Conceptualization. **Yan Zhuge:** Writing – review & editing, Supervision. **Xing Ma:** Writing – review & editing, Supervision. **Milad Bazli:** Writing – review & editing, Supervision. **Allan Manalo:** Writing – review & editing, Supervision.

Declaration of Competing Interest

The authors declare that they have no known competing financial interests or personal relationships that could have appeared to influence the work reported in this paper.

Data availability

Data will be made available on request.

References

[1] Rajak DK, Pagar DD, Menezes PL, Linul E. Fiber-reinforced polymer composites: manufacturing, properties, and applications. Polymers 2019;11:1667.
[2] Nanni A., De Luca A., Zadeh H. Reinforced concrete with FRP bars. Reinforced Concrete with FRP Bars CRC Press, London, United Kingdom doi. 2014;10:b16669.
[3] Gooranorimi O, Nanni A. GFRP reinforcement in concrete after 15 years of service. J Compos Constr 2017;21:04017024.
[4] Younis A, Ebead U, Suraneni P, Nanni A. Cost effectiveness of reinforcement alternatives for a concrete water chlorination tank. J Build Eng 2020;27:100992.
[5] Koch G, Varney J, Thompson N, Moghissi O, Gould M, Payer J. NACE international impact report: international measures of prevention, application, and economics of corrosion technologies study. Houston, TX, USA, Tech Rep: NACE Int; 2016.
[6] Ifrahim MS, Sangi AJ, Ahmad SH. Experimental and numerical investigation of flexural behaviour of concrete beams reinforced with GFRP bars. Struct: Elsevier 2023:104951.
[7] Gouda O, Asadian A, Galal K. Flexural and serviceability behavior of concrete beams reinforced with ribbed GFRP bars. J Compos Constr 2022;26:04022064.
[8] Khorasani AM, Esfahani MR, Sabzi J. The effect of transverse and flexural reinforcement on deflection and cracking of GFRP bar reinforced concrete beams. Compos Part B: Eng 2019;161:530–46.
[9] Al-Sunna R, Pilakoutas K, Hajirasouliha I, Guadagnini M. Deflection behaviour of FRP reinforced concrete beams and slabs: an experimental investigation. Compos Part B: Eng 2012;43:2125–34.
[10] Sheikh SA, Kharal Z. Replacement of steel with GFRP for sustainable reinforced concrete. Constr Build Mater 2018;160:767–74.
[11] Salah-Eldin A, Mohamed HM, Benmokrane B. Effect of GFRP reinforcement ratio on the strength and effective stiffness of high-strength concrete columns: experimental and analytical study. J Compos Constr 2020;24:04020055.
[12] Prajapati GN, Farghaly AS, Benmokrane B. Performance of concrete columns longitudinally reinforced with steel and GFRP bars and confined with GFRP spirals and cross ties under reversed cyclic loading. Eng Struct 2022;270:114863.
[13] Prajapati GN, Farghaly AS, Benmokrane B. Behavior of glass fiber-reinforced polymer-reinforced concrete columns subjected to simulated seismic load. Acids Struct J 2023;120:3–16.
[14] Ma J, Li G-T, Deng X-F, Qian K. Seismic behavior of ultra-high performance concrete columns with GFRP bars under different loading directions. Eng Struct 2023;289:116334.
[15] Paulay T. Joints in Reinforced Concrete Frames Designed Earthquake Resistance. U SN Z-Japan Seminar Report1984.
[16] El-Metwally S, Chen W-F. Structural concrete: strut-and-tie models for unified design. CRC Press; 2017.
[17] El-Naqeeb MH, Hassanli R, Zhuge Y, Ma X, Bazli M, Manalo A. Beam-column connections in GFRP-RC moment resisting frames: A review of seismic behaviour and key parameters. Structures 2025;71:108109.
[18] Hasaballa M, El-Salakawy E. Anchorage performance of GFRP headed and bent bars in beam-column joints subjected to seismic loading. J Compos Constr 2018;22:04018060.
[19] Lin G, Zeng J-J, Liang S-D, Liao J, Zhuge Y. Seismic behavior of novel GFRP bar reinforced concrete beam-column joints internally reinforced with an FRP tube. Eng Struct 2022;273:115100.

[20] Ghomi SK, El-Salakawy E. Effect of joint shear stress on seismic behaviour of interior GFRP-RC beam-column joints. Eng Struct 2019;191:583–97.
[21] Ghomi SK, El-Salakawy E. Seismic behavior of GFRP-reinforced concrete interior beam–column–slab subassemblies. J Compos Constr 2019;23:04019047.
[22] Ghomi SK, El-Salakawy EF. Cyclic Behavior of Glass Fiber-Reinforced Polymer-Reinforced Concrete Exterior Beam-Column-Slab Connections. ACI Structural Journal. 2020;117.
[23] Hopartean G, Donchev T, Petkova D, Georgopoulos C, Limbachiya M. Experimental investigation of concrete frames reinforced with GFRP bars under reversed cyclic loading. Eng Struct 2024;302:117377.
[24] Aliasghar-Mamaghani M, Khaloo A. Seismic behavior of concrete moment frame reinforced with GFRP bars. Compos Part B: Eng 2019;163:324–38.
[25] Hasaballa M, El-Salakawy E. Shear capacity of exterior beam-column joints reinforced with GFRP bars and stirrups. J Compos Constr 2016;20:04015047.
[26] Ghomia SK, El-Salakawy E. Effect of geometrical configuration on seismic behavior of GFRP-RC beam-column joints. Adv Concr Constr 2020;9:313–26.
[27] Elliott KS. Precast concrete structures. Crc Press; 2019.
[28] El-Naqeeb MH, Ghanbari-Ghazijahani T, Gholampour A, Hassanli R, Zhuge Y, Ma X, et al. Cyclic behaviour of an innovative cap beam to column pocketless connection in GFRP-RC precast structures. Structures 2024;61:106003.
[29] Ghanbari-Ghazijahani T, Hassanli R, Manalo A, Smith ST, Vincent T, Gravina R, et al. Cyclic behavior of beam–column pocket connections in GFRP-reinforced precast concrete assemblages. J Compos Constr 2023;27:04022107.
[30] El-Naqeeb MH, Hassanli R, Zhuge Y, Ma X, Manalo A. Numerical investigation on the behaviour of socket connections in GFRP-reinforced precast concrete. Eng Struct 2024;303:117489.
[31] El-Naqeeb MH, Hassanli R, Zhuge Y, Ma X, Bazli M, Manalo A. Performance of GFRP-RC precast cap beam to column connections with epoxy-anchored reinforcement: a numerical study. Arch Civ Mech Eng 2024;24:131.
[32] Hassanli R, Vincent T, Manalo A, Smith ST, Gholampour A, Gravina R, et al. Connections in GFRP reinforced precast concrete frames. Compos Struct 2021;276:114540.
[33] Hassanli R, Vincent T, Manalo A, Smith ST, Gholampour A, Gravina R. Large-scale experimental study on pocket connections in GFRP-reinforced precast concrete frames. Struct: Elsevier 2021:523–41.
[34] Simulia. Simulia. Providence, Rhode Island. 2020.
[35] El-Naqeeb MH, El-Metwally SE, Abdelwahed BS. Performance of exterior beam-column connections with innovative bar anchorage schemes: numerical investigation. Structures 2022;44:534–47.
[36] Caro M, Jemaa Y, Dirar S, Quinn A. Bond performance of deep embedment FRP bars epoxy-bonded into concrete. Eng Struct 2017;147:448–57.
[37] Thorenfeldt E. Mechanical properties of high-strength concrete and applications in design. Symposium Proceedings, Utilization of High-Strength Concrete, Norway, 19871987.
[38] Aslani F, Jowkarmeimandi R. Stress–strain model for concrete under cyclic loading. Mag Concr Res 2012;64:673–85.
[39] Safdar M, Sheikh MN, Hadi MN. Finite element analysis to predict the cyclic performance of GFRP-RC exterior joints with diagonal bars. J Build Eng 2023;65:105774.
[40] Selmy YM, El-Salakawy EF. Numerical investigation on the seismic behaviour of GFRP-reinforced concrete rectangular columns. Eng Struct 2022;262:114355.
[41] Code U.B.. Uniform building code. International Conference of Building Officials, Whittier, CA1997.
[42] Engineers ASoC. Minimum design loads and associated criteria for buildings and other structures. American Society of Civil Engineers; 2017.
[43] Code NRCCACotNB, Code NRCoCACotNB. National building code of Canada: Associate Committee on the National Building Code, National Research Council; 1990.
[44] CSA (Canadian Standards Association). "Design and constructionof building structures with fibre-reinforced polymers.". CAN/CSAS806-12, Rexdale, ON, Canada.; 2012.
[45] Yun H-D, Kim S-H, Choi W. Determination of mechanical properties of sand-coated carbon fiber reinforced polymer (CFRP) rebar. Polymers 2023;15:2186.
[46] Arrayago I, Real E, Gardner L. Description of stress–strain curves for stainless steel alloys. Mater Des 2015;87:540–52.
[47] Hwang I-S, So T-Y, Lee D-H, Shin C-S. Characterization of mechanical properties and grain size of stainless steel 316L via metal powder injection molding. Materials 2023;16:2144.
[48] AS4671. Steel Reinforcing Materials. Standards Australia/Standards New Zealand; 2019.